Journal of Scientific Computing (2024) 100:57
https://doi.org/10.1007/s10915-024-02607-0

A Combined Mixed Hybrid and Hybridizable Discontinuous Galerkin Method for Darcy Flow and Transport

Keegan L. A. Kirk[1] · **Beatrice Riviere**[1]

Received: 29 August 2023 / Revised: 20 June 2024 / Accepted: 21 June 2024

Abstract
A combined hybrid mixed and hybridizable discontinuous Galerkin method is formulated for the flow and transport equations. Convergence of the method is obtained by deriving optimal a priori error bounds in the L^2 norm in space. Since the velocity in the transport equation depends on the flow problem, the stabilization parameter in the HDG method is a function of the discrete velocity. In addition, a key ingredient in the convergence proof is the construction of a projection that is shown to satisfy optimal approximation bounds. Numerical examples confirm the theoretical convergence rates and show the efficiency of high order discontinuous elements.

Keywords Projection operator · H(div)-conformity · A priori error estimates · Hybridization

Mathematics Subject Classification 65M15 · 65M60 · 76S05

1 Introduction

In this article, we formulate and analyze a hybrid mixed–hybridizable discontinuous Galerkin (HM-HDG) method for a one-way coupled flow and transport problem. In particular, we employ a mixed hybrid finite element method for the flow, and HDG for the transport. The highlights of our proposed approach include $H(\text{div})$-conformity of the discrete velocity for the flow problem, optimal rates convergence in *both* the concentration and flux for the transport problem, and hybridization to reduce the size of the global algebraic systems arising from both flow and transport.

✉ Keegan L. A. Kirk
klk12@rice.edu

Beatrice Riviere
riviere@rice.edu

[1] Department of Computational Applied Mathematics and Operations Research, Rice University, Houston, TX 77005, USA

Published online: 08 July 2024

Similar approaches have been taken in [32, 33], where a hybridized Raviart–Thomas method (RT-H) for the flow problem is coupled to the combined RT-H and DG method of Egger and Schöberl [17] for the transport problem; in [31] where an RT-H method for the flow problem is coupled to a local discontinuous Galerkin (LDG) method for the transport problem; in [21] where an RT-H method for the flow problem is coupled to a hybridized finite volume method for the transport problem in the context of fractured porous media; in [20], where the hybridizable LDG (LDG-H) method is applied to *both* the flow and transport problems; and in [6, 7] where a combined hybridized interior penalty (IP-H) method and a hybridized Brezzi–Douglas–Marini (BDM-H) method for the Stokes–Darcy system is coupled to an IP-H method for the transport problem. To highlight how our approach differs from these existing works, let us put them into historical perspective.

Mixed finite element methods have long been applied to porous media flows, as they directly provide an approximation to the flow velocity in addition to the pressure [13, 15, 19, 28, 30]. This is in contrast to primal formulations of the Darcy problem, which provide only an approximation to the pressure and require a post-processing step using numerical differentiation to recover the velocity. However, the saddle-point structure of the flow problem introduces two main challenges to the design of mixed methods. First and foremost, discrete inf-sup stability requires a delicate choice of approximation spaces for the pressure. While a seemingly natural choice would be to balance the degree of the approximation for the velocity and pressure, this choice fails to satisfy a discrete inf-sup condition. This lack of stability can be addressed by either slightly enlarging the velocity space (for instance, RT), or reducing the degree of the pressure approximation (for instance, BDM). Both choices enforce $H(\mathrm{div})$-conformity of the discrete velocity, which is well-known to be beneficial for the transport problem. Second, the resulting algebraic saddle-point problem has an indefinite structure which can be difficult to solve in practice.

To address the problem of indefiniteness, hybridized mixed methods were introduced. Rather than building the $H(\mathrm{div})$-conformity directly into velocity approximation space, once can enforce it by introducing a Lagrange multiplier supported on the mesh skeleton which can be viewed as an approximation to the trace of the pressure. The velocity and pressure can then be statically condensed locally from the algebraic system, resulting in a smaller (positive-definite) global system for only the pressure trace variable on the mesh skeleton. It is well known that the hybridized formulation of the RT and BDM methods produce linear systems algebraically equivalent to their original counterparts (see e.g. [16] and references therein) and thus maintain their desirable properties.

The LDG-H method, on the other hand, strikes a balance between the RT and BDM methods by using equal degree approximations for both the velocity and the pressure. To compensate for the lack of inf-sup stability, a stabilization term is introduced through a numerical flux. Much like the HM methods, the HDG system is closed by enforcing the continuity of the normal component of the *numerical flux* through the introduction of a Lagrange multiplier. A major difference, however, is that the discrete velocity is no longer in $H(\mathrm{div})$. The LDG-H method exhibits optimal rates of convergence for both the velocity and pressure, but it has been well observed that discontinuities in the normal component of the discrete velocity can lead to instabilities when coupled with transport [1].

For this reason, we opt to use a HM method for the flow problem, as $H(\mathrm{div})$-conformity is beneficial for the transport problem. In particular, we follow the approach of [6, 7] and use a BDM-H method for the Darcy flow. We remark that this approach differs from the works [21, 31–33] which use an RT-H method for the flow. While the rate of convergence for the pressure for BDM is one order lower than for RT, there is no coupling between the velocity and pressure errors and thus no overall impact on the rates of convergence for the transport problem. On

the other hand, standard HM methods have difficulties with convection-dominated problems for which LDG-H methods are well-suited. As a DG method, stabilizing mechanisms like upwinding can be built into the numerical flux of LDG-H, with the added benefit of optimal rates of convergence for *both* the flux and the concentration. Comparable accuracy cannot be obtained with the standard DG approaches outlined in the unifying framework of [2].

To perform our error analysis, we leverage the HDG projection introduced in [11] for diffusion equations and extended in [9] to convection-diffusion equations. While this approach is not novel, there is a subtle but important difference between our analysis compared to [8, 9]. In these previous works, the convective velocity is carefully chosen to ensure the underlying convection-diffusion equation is coercive which is essential for the analysis of the HDG projection. In our setting, the flow equations satisfied by the discrete velocity do not provide sufficient control over the divergence of the velocity to guarantee coercivity, and moreover the discrete velocity is discontinuous. This precludes the use of some of the arguments in previous works. Nevertheless, we show that if the source term for the flow problem is essentially bounded, existence and uniqueness of the HDG projection, as well as its optimal approximation properties, can be recovered provided the spatial mesh size is chosen sufficiently small.

The remainder of the article is outlined as follows: in Sect. 2, we introduce the continuous problem and our proposed numerical scheme. In Sect. 3 we summarize known analysis results for our discretization of the flow problem. In Sect. 4, we prove that the algebraic system resulting from our discretization of the transport problem is well-posed, introduce and analyze the HDG projection, and derive optimal error estimates for the transport problem. In Sect. 5, we perform a number of numerical studies to support our theoretical results and investigate the qualitative behaviour of our proposed numerical scheme. Finally, we draw conclusions in Sect. 6.

2 Model Problem and HDG Scheme

Single phase flows in a porous domain $\Omega \subset \mathbb{R}^d$, $d = 2, 3$, over a time interval $(0, T)$ are characterized by the elliptic equations written in a mixed form:

$$\boldsymbol{u} = -\boldsymbol{K}\nabla p, \qquad \text{in } \Omega \times (0, T), \tag{1}$$

$$\operatorname{div}(\boldsymbol{u}) = f, \qquad \text{in } \Omega \times (0, T). \tag{2}$$

where p and $\boldsymbol{u}$ are the fluid pressure and velocity respectively. The symmetric positive definite matrix $\boldsymbol{K}$ represents the permeability field scaled by the inverse of the fluid viscosity, and f is a nonzero source or sink function.

The concentration of a tracer is modeled by the following transport equation, also written in a mixed form:

$$\partial_t c + \operatorname{div}(\boldsymbol{q} + \boldsymbol{u}c) = g, \qquad \text{in } \Omega \times (0, T), \tag{3}$$

$$\boldsymbol{q} = -\boldsymbol{D}\nabla c, \qquad \text{in } \Omega \times (0, T). \tag{4}$$

The diffusion matrix $\boldsymbol{D}$ is a symmetric positive definite matrix and g represents an arbitrary source or sink function. We complement (1–4) with boundary conditions and initial conditions ($\boldsymbol{n}$ denotes the unit normal vector outward to Ω):

$$\boldsymbol{u} \cdot \boldsymbol{n} = 0, \quad \text{on } \partial\Omega \times (0, T), \tag{5}$$

$$\boldsymbol{q} \cdot \boldsymbol{n} = 0, \quad \text{on } \partial\Omega \times (0, T), \tag{6}$$

$$c = c_0, \quad \text{in } \partial\Omega \times \{0\}. \tag{7}$$

Thanks to the homogeneous Neumann boundary conditions on the pressure and to ensure the problem is well-posed, we require

$$\int_\Omega f = \int_\Omega p = 0. \tag{8}$$

Next, we discretize (1–4) with the hybrizable discontinuous Galerkin method. Let $\mathcal{E}_h$ be a conforming shape-regular mesh of Ω that consists of simplices E with boundary ∂E and outward unit normal vector $\boldsymbol{n}_E$. As usual, the mesh size h is the maximum of the element diameter h_E over all elements E. We denote by $\partial\mathcal{E}_h$ the union of the faces, namely $\partial\mathcal{E}_h = \cup_{E\in\mathcal{E}_h}\partial E$.

Let $k \geq 1$ be a fixed integer. The space of discontinuous polynomials of degree k is denoted by $\mathcal{P}_k$:

$$\mathcal{P}_k = \{w \in L^2(\Omega) : w|_E \in \mathbb{P}_k(E),\ \forall E \in \mathcal{E}_h\}.$$

The discrete HDG spaces are:

$$\begin{aligned} \boldsymbol{V}_h =& (\mathcal{P}_k)^d, \quad W_h = \mathcal{P}_k, \quad Q_h = \mathcal{P}_{k-1}, \\ M_h =& \{\widehat{w}_h \in L^2(\partial\mathcal{E}_h) : \widehat{w}_h|_e \in \mathbb{P}_k(e),\ \forall e \in \partial\mathcal{E}_h\}. \end{aligned}$$

For readability, we denote by $(\cdot,\cdot)_E$ the L^2 inner-product on an element E and by $\langle\cdot,\cdot\rangle_e$ the L^2 inner-product on a face $e \subset \partial E$. We also define

$$(w, v)_{\mathcal{E}_h} = \sum_{E\in\mathcal{E}_h} (w, v)_E, \quad \langle w, v\rangle_{\partial\mathcal{E}_h} = \sum_{E\in\mathcal{E}_h} \langle w, v\rangle_{\partial E}, \tag{9}$$

with the usual modifications for vector-valued functions. Let $\tau > 0$ be the time step value and let $t^n = n\tau$ be the n-th discrete time such that $0 < t^1 < \cdots < t^N = T$ is a uniform partition of the time interval.

The fully discrete HM-HDG method reads: first find $(\boldsymbol{u}_h, p_h, \widehat{p}_h) \in \boldsymbol{V}_h \times (Q_h \cap L^2_0(\Omega)) \times M_h$ such that

$$\forall \boldsymbol{v}_h \in \boldsymbol{V}_h, \quad (\boldsymbol{K}^{-1}\boldsymbol{u}_h, \boldsymbol{v}_h)_{\mathcal{E}_h} - (p_h, \nabla\cdot\boldsymbol{v}_h)_{\mathcal{E}_h} + \langle\widehat{p}_h, \boldsymbol{v}_h\cdot\boldsymbol{n}\rangle_{\partial\mathcal{E}_h} = 0, \tag{10a}$$

$$\forall w_h \in Q_h \cap L^2_0(\Omega), \quad (\nabla\cdot\boldsymbol{u}_h, w_h)_{\mathcal{E}_h} = (f, w_h)_{\mathcal{E}_h}, \tag{10b}$$

$$\forall \widehat{w}_h \in M_h, \quad \langle\boldsymbol{u}_h\cdot\boldsymbol{n}, \widehat{w}_h\rangle_{\partial\mathcal{E}_h} = 0. \tag{10c}$$

Next, for $1 \leq n \leq N$, given $c_h^{n-1} \in W_h$, find $(\boldsymbol{q}_h^n, c_h^n, \widehat{c}_h^n) \in \boldsymbol{V}_h \times W_h \times M_h$ satisfying

$$\forall \boldsymbol{v}_h \in \boldsymbol{V}_h, \quad (\boldsymbol{D}^{-1}\boldsymbol{q}_h^n, \boldsymbol{v}_h)_{\mathcal{E}_h} - (c_h^n, \nabla\cdot\boldsymbol{v}_h)_{\mathcal{E}_h} + \langle\widehat{c}_h^n, \boldsymbol{v}_h\cdot\boldsymbol{n}\rangle_{\partial\mathcal{E}_h} = 0, \tag{11a}$$

$$\begin{aligned} \forall w_h \in W_h, \quad & \frac{1}{\tau}(c_h^n - c_h^{n-1}, w_h)_{\mathcal{E}_h} - (\boldsymbol{u}_h c_h^n + \boldsymbol{q}_h^n, \nabla w_h)_{\mathcal{E}_h} \\ & + \langle(\boldsymbol{q}_h^n + \boldsymbol{u}_h\widehat{c}_h^n)\cdot\boldsymbol{n} + \sigma(c_h^n - \widehat{c}_h^n), w_h\rangle_{\partial\mathcal{E}_h} = (g, w_h)_{\mathcal{E}_h}, \end{aligned} \tag{11b}$$

$$\forall \widehat{w}_h \in M_h, \quad \langle(\boldsymbol{q}_h^n + \boldsymbol{u}_h\widehat{c}_h^n)\cdot\boldsymbol{n} + \sigma(c_h^n - \widehat{c}_h^n), \widehat{w}_h\rangle_{\partial\mathcal{E}_h} = 0. \tag{11c}$$

The stabilization function σ in the numerical flux is chosen following the considerations in [20, 25]:

$$\sigma|_{\partial E} = |\boldsymbol{u}_h\cdot\boldsymbol{n}_E| + \max(\|\boldsymbol{D}\|_{L^\infty(\Omega)}, 1), \quad \forall E \in \mathcal{E}_h. \tag{12}$$

The vector $\boldsymbol{n}_E$ denotes the unit normal vector outward of ∂E. We initialize the scheme with the L^2-projection of the initial data into W_h, i.e. $c_h^0 = \pi_k c_0$, where π_k denotes the L^2 operator

defined by:

$$\forall w \in L^2(\Omega), \quad \forall w_h \in W_h, \quad (\pi_k w, w_h)_{\mathcal{E}_h} = (w, w_h)_{\mathcal{E}_h}. \tag{13}$$

Since $f \in L_0^2(\Omega)$ and $\boldsymbol{u}_h \cdot \boldsymbol{n} = 0$ on $\partial\Omega$, it is easy to check that (10b) is satisfied for $w_h \in Q_h$.

We will also make use of the L^2 projection operator $\widehat{\pi_k}$ over the mesh skeleton, defined by:

$$\forall w \in L^2(\partial\mathcal{E}_h), \quad \forall \widehat{w}_h \in M_h, \quad \forall e \in \partial\mathcal{E}_h, \quad \langle \widehat{\pi_k w}, \widehat{w}_h \rangle_e = \langle w, \widehat{w}_h \rangle_e. \tag{14}$$

The L^2 projections satisfy the following approximation properties for positive constants C and C_∞ independent of h_E and h [3, 18]:

$$\forall E \in \mathcal{E}_h, \quad \forall w \in H^{k+1}(E), \quad \|w - \pi_{k-1} w\|_{L^2(E)} \leq C h_E^k |w|_{H^{k+1}(E)}, \tag{15}$$

$$\forall E \in \mathcal{E}_h, \quad \forall w \in H^{k+1}(E), \quad \|w - \widehat{\pi_k w}\|_{L^2(\partial E)} \leq C h_E^{k+1/2} |w|_{H^{k+1}(E)}, \tag{16}$$

$$\forall w \in L^\infty(\Omega), \quad \|\pi_{k-1} w\|_{L^\infty(\Omega)} \leq C_\infty \|w\|_{L^\infty(\Omega)}. \tag{17}$$

3 Analysis of the Scheme

The one-way coupling of the flow with transport allows us to treat the flow equations separately from the transport equations.

3.1 Flow Problem

Since Problem (10) is a well-known numerical method that originates from [5] in 2D and [4, 24] in 3D and that has been studied in e.g. [16], we state the results without providing a proof. Well-posedness is shown in detail in [16, Section 2.4].

An important tool for the derivation of error bounds for the flow problem is the BDM projection [3, 16], defined locally, for a vector function $\boldsymbol{q}$ sufficiently smooth, as:

$$\forall \boldsymbol{v}_h \in \mathcal{N}_{k-2}(E), \quad (\boldsymbol{\Pi}^{\mathrm{BDM}} \boldsymbol{q}, \boldsymbol{v}_h)_E = (\boldsymbol{q}, \boldsymbol{v}_h)_E, \tag{18a}$$

$$\forall \widehat{w}_h \in \mathcal{R}(\partial E), \quad \langle \boldsymbol{\Pi}^{\mathrm{BDM}} \boldsymbol{q} \cdot \boldsymbol{n}, \widehat{w}_h \rangle_{\partial E} = \langle \boldsymbol{q} \cdot \boldsymbol{n}, \widehat{w}_h \rangle_{\partial E}, \tag{18b}$$

where $\mathcal{N}_{k-2}(E)$ is the local Nédélec space of the first kind [3, 23] and $\mathcal{R}_k(\partial E)$ is the restriction of M_h to a single element E. The following commutativity property holds, for any $E \in \mathcal{E}_h$:

$$\nabla \cdot \boldsymbol{\Pi}^{\mathrm{BDM}} \boldsymbol{q} = \pi_{k-1} \nabla \cdot \boldsymbol{q}, \quad \text{on } E. \tag{19}$$

In addition, there exists a constant $C > 0$ such that, for $1 \leq m \leq k+1$, for $E \in \mathcal{E}_h$ and any $\boldsymbol{q} \in (H^m(E))^d$, we have

$$\left\| \boldsymbol{q} - \boldsymbol{\Pi}^{\mathrm{BDM}} \boldsymbol{q} \right\|_{L^2(E)} \leq C h^m |\boldsymbol{q}|_{H^m(E)}. \tag{20}$$

The starting point of the analysis is the error equations. For this, we introduce the following notation:

$$\begin{aligned} &e_{\boldsymbol{u}} = \boldsymbol{u} - \boldsymbol{u}_h, \quad \zeta_{\boldsymbol{u}} = \boldsymbol{\Pi}^{\mathrm{BDM}} \boldsymbol{u} - \boldsymbol{u}_h, \quad \xi_{\boldsymbol{u}} = \boldsymbol{u} - \boldsymbol{\Pi}^{\mathrm{BDM}} \boldsymbol{u}, \\ &e_p = p - p_h, \quad \zeta_p = \pi_{k-1} p - p_h, \quad \xi_p = p - \pi_{k-1} p, \\ &\widehat{e}_p = p - \widehat{p}_h, \quad \widehat{\zeta}_p = \widehat{\pi_k p} - \widehat{p}_h, \quad \widehat{\xi}_p = p - \widehat{\pi_k p}. \end{aligned}$$

Lemma 1 (Darcy error equations)

$$(\boldsymbol{K}^{-1} \zeta_{\boldsymbol{u}}, \boldsymbol{v}_h)_{\mathcal{E}_h} - (\zeta_p, \nabla \cdot \boldsymbol{v}_h)_{\mathcal{E}_h} + \langle \widehat{\zeta}_p, \boldsymbol{v}_h \cdot \boldsymbol{n} \rangle_{\partial \mathcal{E}_h} = -(\boldsymbol{K}^{-1} \xi_{\boldsymbol{u}}, \boldsymbol{v}_h)_{\mathcal{E}_h}, \tag{21a}$$

$$(\nabla \cdot \zeta_{\boldsymbol{u}}, w_h)_{\mathcal{E}_h} = 0, \tag{21b}$$

$$\langle \zeta_{\boldsymbol{u}} \cdot \boldsymbol{n}, \widehat{w}_h \rangle_{\partial \mathcal{E}_h} = 0, \tag{21c}$$

for all $(\boldsymbol{v}_h, w_h, \widehat{w}_h) \in \boldsymbol{V}_h \times Q_h \times M_h$.

Next, using the error equations above, we obtain local bounds.

Lemma 2 *There exists a constant* $C > 0$ *independent of* h_E *such that the following bounds hold:*

$$\forall E \in \mathcal{E}_h, \quad \left\| \boldsymbol{K}^{-1/2} \zeta_{\boldsymbol{u}} \right\|_{L^2(E)} \leq \left\| \boldsymbol{K}^{-1/2} \xi_{\boldsymbol{u}} \right\|_{L^2(E)}, \tag{22}$$

$$\forall E \in \mathcal{E}_h, \quad h_E^{1/2} \| \zeta_{\boldsymbol{u}} \cdot \boldsymbol{n} \|_{L^2(\partial E)} \leq C \left\| \xi_{\boldsymbol{u}} \right\|_{L^2(E)}. \tag{23}$$

Using the fact that the pair of spaces $(H_0^1(\Omega))^d \times L_0^2(\Omega)$ satisfies an inf-sup condition [22], we derive the following bound on ζ_p:

Lemma 3 *There exists a constant* $C > 0$ *independent of* h *such that*

$$\| \zeta_p \|_{L^2(\Omega)} \leq C \left\| e_{\boldsymbol{u}} \right\|_{L^2(\Omega)}. \tag{24}$$

Finally, we have the following local bound on $\widehat{\zeta}_p$.

Lemma 4 *There exists a constant* $C > 0$ *independent of* h *and* h_E *such that*

$$\forall E \in \mathcal{E}_h, \quad \left\| \widehat{\zeta}_p \right\|_{L^2(E)} \leq C \left(h_E^{-1/2} \| \zeta_p \|_{L^2(E)} + h_E^{1/2} \| e_{\boldsymbol{u}} \|_{L^2(E)} \right). \tag{25}$$

An immediate consequence of (15), (16), (20) and Lemmas 2–4 is the following a priori estimates for the Darcy problem:

Theorem 1 *Suppose that* $k \geq 1$ *and* $(\boldsymbol{u}, p) \in (H^{k+1}(\Omega))^d \times H^{k+1}(\Omega)$ *solves the Darcy problem* (1) *and* $(\boldsymbol{u}_h, p_h, \widehat{p}_h)$ *solves the discrete Darcy problem* (10). *There exists a constant* $C > 0$ *such that, for all* $E \in \mathcal{E}_h$,

$$\| \boldsymbol{u} - \boldsymbol{u}_h \|_{L^2(E)} \leq C h_E^{k+1} |\boldsymbol{u}|_{H^{k+1}(E)}, \tag{26a}$$

$$\| p - p_h \|_{L^2(\Omega)} \leq C h^k (|p|_{H^{k+1}(\Omega)} + |\boldsymbol{u}|_{H^{k+1}(\Omega)}), \tag{26b}$$

$$\| (\boldsymbol{u} - \boldsymbol{u}_h) \cdot \boldsymbol{n} \|_{L^2(\partial E)} \leq C h_E^{k+1/2} |\boldsymbol{u}|_{H^{k+1}(E)}, \tag{26c}$$

If in addition, the mesh is quasi-uniform, we have

$$\| p - \widehat{p}_h \|_{L^2(\partial \mathcal{E}_h)} \leq C h^{k+1/2} (|p|_{H^{k+1}(\Omega)} + |\boldsymbol{u}|_{H^{k+1}(\Omega)}). \tag{27}$$

Using a standard inverse inequality (locally on one element) and a Sobolev embedding, we derive the following uniform L^∞ bound on the discrete Darcy velocity $\boldsymbol{u}_h$:

Corollary 1 *Assume that the velocity solution to the Darcy problem* (1) *satisfies* $\boldsymbol{u} \in (H^2(\Omega))^d$. *Then, there exists a constant* $C > 0$, *independent of the mesh size* h, *such that*

$$\| \boldsymbol{u}_h \|_{L^\infty(\Omega)} \leq C \| \boldsymbol{u} \|_{H^2(\Omega)}. \tag{28}$$

Remark 1 Theorem 1 shows that using a lower order approximation for the pressure will not impact the accuracy of the proposed HDG method for the transport problem. Thus, the use of the BDM-H scheme over the RT-H scheme may be more desirable from the point of view of implementation. However, if one desires a more accurate pressure approximation, the following local post-processing scheme from [29] can be applied efficiently in an element-by-element fashion: find $p_h^\star \in \mathbb{P}_{k+1}(E)$ satisfying for all $w_h \in \mathbb{P}_{k+1}(E)$ the system:

$$-(\boldsymbol{K}\nabla p_h^\star, \nabla w_h)_E = (\boldsymbol{u}_h, \nabla w_h)_E, \tag{29a}$$

$$(p_h^\star, 1)_E = (p_h, 1)_E. \tag{29b}$$

It is well-known (see, e.g. [29, Theorem 2.2]) that $p_h^\star$ converges with order $k+2$ if $k \geq 2$ and order $k+1$ if $k = 1$.

Remark 2 Our motivation for considering a HM method for the Darcy flow problem is the $H(\mathrm{div}; \Omega)$-conformity of the velocity approximation. However, if one wishes to use the HDG method for *both* flow and transport, the velocity approximation may be post-processed in an element-by-element fashion to obtain an $H(\mathrm{div}; \Omega)$-conforming velocity approximation (see, e.g. [12] for further details).

3.2 Bound on the Divergence of the Discrete Velocity

For the well-posedness of the discrete transport problem (11) as well as for the error analysis in the sequel, we require an L^∞-bound on the divergence of the approximate Darcy velocity. Such a bound follows immediately from the following lemma:

Lemma 5 *Let $\boldsymbol{u}_h \in \boldsymbol{V}_h$ be the unique solution to the discrete Darcy flow problem (10). Then, $\boldsymbol{u}_h$ belongs to $H_0(\mathrm{div}; \Omega)$ and*

$$\nabla \cdot \boldsymbol{u}_h = \pi_{k-1} f. \tag{30}$$

Proof To show that $\boldsymbol{u}_h$ belongs to $H_0(\mathrm{div}; \Omega)$, it suffices to prove the continuity of the normal component of $\boldsymbol{u}_h$ across the interior faces of the mesh skeleton $\partial\mathcal{E}_h$, and that $\boldsymbol{u}_h \cdot \boldsymbol{n} = 0$ on the boundary $\partial\Omega$. This is easily obtained by choosing $\widehat{w}_h$ in (10c) to be zero everywhere except on one face $e \subset \partial\mathcal{E}_h$. Equation (30) follows immediately from (10b). □

Remark 3 Alternative to the hybridized mixed methods, one could instead approximate the Darcy problem using the hybridizable discontinuous Galerkin method as done in [20]. This, however, presents a number of challenges

4 Analysis of the Transport Problem

4.1 Existence and Uniqueness of the Discrete Solution

We now demonstrate that the transport problem (11) is well-posed under assumptions that depend on the regularity of the source/sink function f in (2).

Assumption A The function f belongs to $L^\infty(\Omega)$ and τ is chosen small enough, namely $\tau \leq \tau_0$, with

$$\tau_0 = \frac{1}{C_\infty \|f\|_{L^\infty(\Omega)}},$$

where C_∞ is the constant in (17).

To prove well-posedness of the transport problem, since we are dealing with a square linear system in finite dimensions, it suffices to prove the corresponding homogeneous problem has only the trivial solution.

Lemma 6 *Let Assumption A hold true. Given $\boldsymbol{u}_h \in \boldsymbol{V}_h$ satisfying the discrete Darcy flow problem (10), $(\boldsymbol{q}_h, c_h, \widehat{c}_h) = (\boldsymbol{0}, 0, 0)$ is the unique solution to the homogeneous system*

$$(\boldsymbol{D}^{-1}\boldsymbol{q}_h, \boldsymbol{v}_h)_{\mathcal{E}_h} - (c_h, \nabla\cdot\boldsymbol{v}_h)_{\mathcal{E}_h} + \langle\widehat{c}_h, \boldsymbol{v}_h\cdot\boldsymbol{n}\rangle_{\partial\mathcal{E}_h} = 0, \tag{31a}$$

$$\begin{aligned}(c_h, w_h)_{\mathcal{E}_h} - \tau(\boldsymbol{u}_h c_h + \boldsymbol{q}_h, \nabla w_h)_{\mathcal{E}_h} + \tau\langle(\boldsymbol{q}_h + \boldsymbol{u}_h\widehat{c}_h)\cdot\boldsymbol{n}, w_h\rangle_{\partial\mathcal{E}_h}\\ + \tau\langle\sigma(c_h - \widehat{c}_h), w_h\rangle_{\partial\mathcal{E}_h} = 0,\end{aligned} \tag{31b}$$

$$\langle(\boldsymbol{q}_h + \boldsymbol{u}_h\widehat{c}_h)\cdot\boldsymbol{n}, \widehat{w}_h\rangle_{\partial\mathcal{E}_h} + \langle\sigma(c_h - \widehat{c}_h), \widehat{w}_h\rangle_{\partial\mathcal{E}_h} = 0, \tag{31c}$$

for all $(\boldsymbol{v}_h, w_h, \widehat{w}_h) \in \boldsymbol{V}_h \times W_h \times M_h$.

Proof We first choose $\boldsymbol{v}_h = \tau\boldsymbol{q}_h$ in (31a) and integrate by parts to find

$$\tau(\boldsymbol{D}^{-1}\boldsymbol{q}_h, \boldsymbol{q}_h)_{\mathcal{E}_h} + \tau(\nabla c_h, \boldsymbol{q}_h)_{\mathcal{E}_h} - \tau\langle c_h - \widehat{c}_h, \boldsymbol{q}_h\cdot\boldsymbol{n}\rangle_{\partial\mathcal{E}_h} = 0. \tag{32}$$

Next, we choose $w_h = c_h$ in (31b):

$$\begin{aligned}\|c_h\|^2_{L^2(\Omega)} - \tau(\boldsymbol{u}_h c_h + \boldsymbol{q}_h, \nabla c_h)_{\mathcal{E}_h} + \tau\langle(\boldsymbol{q}_h + \boldsymbol{u}_h\widehat{c}_h)\cdot\boldsymbol{n}, c_h\rangle_{\partial\mathcal{E}_h}\\ + \tau\langle\sigma(c_h - \widehat{c}_h), c_h\rangle_{\partial\mathcal{E}_h} = 0.\end{aligned}$$

Summing these two equations, we have

$$\begin{aligned}\|c_h\|^2_{L^2(\Omega)} + \tau(\boldsymbol{D}^{-1}\boldsymbol{q}_h, \boldsymbol{q}_h)_{\mathcal{E}_h} + \tau\langle\widehat{c}_h, \boldsymbol{q}_h\cdot\boldsymbol{n}\rangle_{\partial\mathcal{E}_h} - \tau(\boldsymbol{u}_h c_h, \nabla c_h)_{\mathcal{E}_h}\\ + \tau\langle\boldsymbol{u}_h\widehat{c}_h\cdot\boldsymbol{n}, c_h\rangle_{\partial\mathcal{E}_h} + \tau\langle\sigma(c_h - \widehat{c}_h), c_h\rangle_{\partial\mathcal{E}_h} = 0.\end{aligned} \tag{33}$$

Choosing $\widehat{w}_h = -\tau\widehat{c}_h$ in (31c) and adding the resulting equation to (33) yields

$$\begin{aligned}\|c_h\|^2_{L^2(\Omega)} + \tau(\boldsymbol{D}^{-1}\boldsymbol{q}_h, \boldsymbol{q}_h)_{\mathcal{E}_h} - \tau(\boldsymbol{u}_h c_h, \nabla c_h)_{\mathcal{E}_h}\\ + \tau\langle\boldsymbol{u}_h\cdot\boldsymbol{n}\widehat{c}_h, c_h - \widehat{c}_h\rangle_{\partial\mathcal{E}_h} + \tau\langle\sigma(c_h - \widehat{c}_h), c_h - \widehat{c}_h\rangle_{\partial\mathcal{E}_h} = 0.\end{aligned} \tag{34}$$

Adding and subtracting $\tau\langle\boldsymbol{u}_h\cdot\boldsymbol{n}c_h, c_h - \widehat{c}_h\rangle_{\partial\mathcal{E}_h}$, we find

$$\begin{aligned}\|c_h\|^2_{L^2(\Omega)} + \tau(\boldsymbol{D}^{-1}\boldsymbol{q}_h, \boldsymbol{q}_h)_{\mathcal{E}_h} - \tau(\boldsymbol{u}_h c_h, \nabla c_h)_{\mathcal{E}_h}\\ + \tau\langle(\sigma - \boldsymbol{u}_h\cdot\boldsymbol{n})(c_h - \widehat{c}_h), c_h - \widehat{c}_h\rangle_{\partial\mathcal{E}_h} + \tau\langle\boldsymbol{u}_h\cdot\boldsymbol{n}c_h, c_h - \widehat{c}_h\rangle_{\partial\mathcal{E}_h} = 0.\end{aligned}$$

Next, using the fact that $\boldsymbol{u}_h c_h\cdot\nabla c_h = \frac{1}{2}\nabla\cdot(\boldsymbol{u}_h c_h^2) - \frac{1}{2}c_h^2\nabla\cdot\boldsymbol{u}_h$ on each element, we apply Gauss's theorem element-by-element to find

$$-\tau(\boldsymbol{u}_h c_h, \nabla c_h)_{\mathcal{E}_h} = \frac{\tau}{2}((\nabla\cdot\boldsymbol{u}_h)c_h, c_h)_{\mathcal{E}_h} - \frac{\tau}{2}\langle\boldsymbol{u}_h\cdot\boldsymbol{n}c_h, c_h\rangle_{\partial\mathcal{E}_h},$$

so that, after some algebraic manipulations, and using the fact that $\boldsymbol{u}_h\cdot\boldsymbol{n}$ and $\widehat{c}_h$ are both single-valued across element boundaries and that $\boldsymbol{u}_h\cdot\boldsymbol{n}|_{\partial\Omega} = 0$, we arrive at

$$\begin{aligned}\|c_h\|^2_{L^2(\Omega)} + \tau(\boldsymbol{D}^{-1}\boldsymbol{q}_h, \boldsymbol{q}_h)_{\mathcal{E}_h} + \frac{\tau}{2}((\nabla\cdot\boldsymbol{u}_h)c_h, c_h)_{\mathcal{E}_h}\\ + \tau\langle(\sigma - \frac{1}{2}\boldsymbol{u}_h\cdot\boldsymbol{n})(c_h - \widehat{c}_h), c_h - \widehat{c}_h\rangle_{\partial\mathcal{E}_h} = 0.\end{aligned} \tag{35}$$

Next, we rearrange, use the fact that $\nabla\cdot\boldsymbol{u}_h = \pi_{k-1}f$ to find (note that $\sigma - \frac{1}{2}\boldsymbol{u}_h\cdot\boldsymbol{n} > 0$)

$$\tau(\boldsymbol{D}^{-1}\boldsymbol{q}_h, \boldsymbol{q}_h)_{\mathcal{E}_h} + \|c_h\|^2_{L^2(\Omega)} + \tau\langle(\sigma - \frac{1}{2}\boldsymbol{u}_h\cdot\boldsymbol{n})(c_h - \widehat{c}_h), c_h - \widehat{c}_h\rangle_{\partial\mathcal{E}_h}$$

$$\leq \frac{\tau}{2}|((\pi_{k-1}f)c_h, c_h)_{\mathcal{E}_h}|. \tag{36}$$

With Assumption A, we write

$$\begin{aligned}&\tau(\boldsymbol{D}^{-1}\boldsymbol{q}_h, \boldsymbol{q}_h)_{\mathcal{E}_h} + \|c_h\|^2_{L^2(\Omega)} + \tau\langle(\sigma - \frac{1}{2}\boldsymbol{u}_h\cdot\boldsymbol{n})(c_h - \widehat{c}_h), c_h - \widehat{c}_h\rangle_{\partial\mathcal{E}_h}\\ &\leq \frac{\tau}{2}\|\pi_{k-1}f\|_{L^\infty(\Omega)}\|c_h\|^2_{L^2(\Omega)} \leq \frac{\tau}{2}C_\infty\|f\|_{L^\infty(\Omega)}\|c_h\|^2_{L^2(\Omega)}.\end{aligned}$$

Therefore, since $\tau \leq \tau_0$, we can conclude that $\boldsymbol{q}_h = \boldsymbol{0}$, $c_h = 0$, and $\widehat{c}_h = 0$. □

4.2 Error Analysis for the Transport Problem

4.2.1 The HDG Projection

Motivated by the analysis in [9], on any simplex $E \in \mathcal{E}_h$ we define a projection $\boldsymbol{\Pi}^{\mathrm{HDG}}(\boldsymbol{q}, c) = (\boldsymbol{\Pi}_V\boldsymbol{q}, \Pi_W c)$, dependent on the discrete Darcy velocity $\boldsymbol{u}_h$ obtained from (10), as the element of $(\mathbb{P}_k(E))^d \times \mathbb{P}_k(E)$ solving the equations

$$\forall \boldsymbol{v}_h \in (\mathbb{P}_{k-1}(E))^d, \quad (\boldsymbol{\Pi}_V\boldsymbol{q} + \boldsymbol{u}_h\Pi_W c, \boldsymbol{v}_h)_E = (\boldsymbol{q} + \boldsymbol{u}c, \boldsymbol{v}_h)_E, \tag{37a}$$

$$\forall w_h \in \mathbb{P}_{k-1}(E), \quad (\Pi_W c, w_h)_E = (c, w_h)_E, \tag{37b}$$

$$\begin{aligned}&\forall e \subset \partial E,\ \forall \widehat{w}_h \in \mathbb{P}_k(e),\ \langle\boldsymbol{\Pi}_V\boldsymbol{q}\cdot\boldsymbol{n} + \sigma\Pi_W c, \widehat{w}_h\rangle_e = \langle\boldsymbol{q}\cdot\boldsymbol{n} + \boldsymbol{u}\cdot\boldsymbol{n}c, \widehat{w}_h\rangle_e\\ &\quad + \langle\sigma c - \boldsymbol{u}_h\cdot\boldsymbol{n}\widehat{\pi_k c}, \widehat{w}_h\rangle_e.\end{aligned} \tag{37c}$$

To analyze this projection, we require the following lemma taken from [9, 11]:

Lemma 7 *Denote by $\mathbb{P}_k^\perp(E)$ the orthogonal complement of $\mathbb{P}_{k-1}(E)$ in $\mathbb{P}_k(E)$, that is,*

$$\mathbb{P}_k^\perp(E) = \{w_h \in \mathbb{P}_k(E) \mid (w_h, v_h)_E = 0,\ \forall v_h \in \mathbb{P}_{k-1}(E)\}. \tag{38}$$

For all $w_h \in P_k^\perp(E)$, there exists a constant $C_* > 0$ such that

$$\|w_h\|_{L^2(E)} \leq C_* h_E^{1/2}\|w_h\|_{L^2(e)}, \tag{39}$$

for any face $e \subset \partial E$.

First, it is easy to check that (37a–37c) yields a square linear system, thus existence is equivalent to uniqueness. Indeed, we observe that

$$\dim\mathbb{P}_k(E) = \frac{(k+d)!}{d!\,k!}, \quad \dim\mathbb{P}_k(e) = \frac{(k+d-1)!}{(d-1)!\,k!}.$$

Thus, the dimension of $(\mathbb{P}_k(E))^d \times \mathbb{P}_k(E)$ is

$$\dim(\mathbb{P}_k(E))^d + \dim\mathbb{P}_k(E) = \frac{(d+1)(k+d)!}{d!\,k!},$$

while the number of equations defining the HDG projection is equal to

$$\begin{aligned}&\dim(\mathbb{P}_{k-1}(E))^d + \dim \mathbb{P}_{k-1}(E) + (d+1)\dim \mathbb{P}_k(e)\\ &= \frac{(d+1)(k+d-1)!}{d!\,(k-1)!} + \frac{(d+1)(k+d-1)!}{(d-1)!\,k!}\\ &= \frac{(d+1)(k+d)(k+d-1)!}{d!\,k!} = \dim(\mathbb{P}_k(E))^d + \dim \mathbb{P}_k(E).\end{aligned}$$

To prove uniqueness, let $\delta_{\boldsymbol{q}}$ and δ_c denote the difference between two projections. They satisfy

$$\forall \boldsymbol{v}_h \in (\mathbb{P}_{k-1}(E))^d, \quad (\delta_{\boldsymbol{q}} + \boldsymbol{u}_h \delta_c, \boldsymbol{v}_h)_E = 0, \tag{40}$$

$$\forall w_h \in \mathbb{P}_{k-1}(E), \quad (\delta_c, w_h)_E = 0, \tag{41}$$

$$\forall e \subset \partial E,\ \forall \widehat{w}_h \in \mathbb{P}_k(e), \quad \langle \delta_{\boldsymbol{q}} \cdot \boldsymbol{n} + \sigma \delta_c, \widehat{w}_h \rangle_e = 0. \tag{42}$$

From (41), we see that δ_c belongs to $\mathbb{P}_k^{\perp}(E)$. Choose $\widehat{w}_h = \delta_c|_e$ for all $e \subset \partial E$, and sum over all e:

$$\langle \sigma \delta_c, \delta_c \rangle_{\partial E} = -(\nabla \cdot \delta_{\boldsymbol{q}}, \delta_c)_E - (\delta_{\boldsymbol{q}}, \nabla \delta_c)_E$$

Since $\nabla \cdot \delta_{\boldsymbol{q}}$ belongs to $\mathbb{P}_{k-1}$, we have

$$\langle \sigma \delta_c, \delta_c \rangle_{\partial E} = -(\delta_{\boldsymbol{q}}, \nabla \delta_c)_E$$

Choosing $\boldsymbol{v}_h = \nabla \delta_c$ in (40) yields

$$\langle \sigma \delta_c, \delta_c \rangle_{\partial E} = (\boldsymbol{u}_h \delta_c, \nabla \delta_c)_E = \frac{1}{2}\langle \boldsymbol{u}_h \cdot \boldsymbol{n}\, \delta_c, \delta_c \rangle_{\partial E} - \frac{1}{2}((\nabla \cdot \boldsymbol{u}_h)\delta_c, \delta_c)_E.$$

Therefore,

$$\langle (\sigma - \frac{1}{2}\boldsymbol{u}_h \cdot \boldsymbol{n})\, \delta_c, \delta_c \rangle_{\partial E} \le \frac{1}{2}\|\pi_{k-1} f\|_{L^\infty(\Omega)} \|\delta_c\|^2_{L^2(E)} \le \frac{1}{2} C_\infty \|f\|_{L^\infty(\Omega)} \|\delta_c\|^2_{L^2(E)}.$$

By (12), we have

$$\sigma - \frac{1}{2}\boldsymbol{u}_h \cdot \boldsymbol{n} \ge 1. \tag{43}$$

Thus, with (39) we obtain

$$\begin{aligned}\|\delta_c\|^2_{L^2(E)} \le C_* h_E \|\delta_c\|^2_{L^2(\partial E)} &\le C_* h_E \langle (\sigma - \frac{1}{2}\boldsymbol{u}_h \cdot \boldsymbol{n})\, \delta_c, \delta_c \rangle_{\partial E}\\ &\le C_* h_E \frac{1}{2} C_\infty \|f\|_{L^\infty(\Omega)} \|\delta_c\|^2_{L^2(E)}.\end{aligned}$$

Therefore, assuming that

$$C_* h_E C_\infty \|f\|_{L^\infty(\Omega)} \le 1,$$

we may conclude that $\delta_c = 0$. This implies that component-wise $\delta_{\boldsymbol{q}}$ belongs to $\mathbb{P}_k^{\perp}$ and that $\delta_{\boldsymbol{q}} \cdot \boldsymbol{n} = 0$ on ∂E. With (39), we conclude that $\delta_{\boldsymbol{q}} = \boldsymbol{0}$. Define

$$h_0 = \frac{1}{C_* C_\infty \|f\|_{L^\infty(\Omega)}}. \tag{44}$$

Then for all $h \le h_0$ the functions $\Pi_V \boldsymbol{q}$ and $\Pi_W c$ exist and are unique.

We remark that, thanks to Corollary 1, the approximation errors derived below for the projection $\boldsymbol{\Pi}^{\mathrm{HDG}}$ are independent of $\boldsymbol{u}_h$ assuming the exact Darcy velocity is sufficiently regular, i.e. $\boldsymbol{u} \in (H^2(\Omega))^d$.

The following proposition is similar to [9, Proposition 4.2]. We reproduce the proof below.

Proposition 1 *The component $\Pi_W c$ of the HDG projection defined in (37) satisfies for all $z_h \in \mathbb{P}_k^{\perp}(E)$,*

$$\begin{aligned}\langle \sigma(\Pi_W c - c), z_h\rangle_{\partial E} &= (\nabla\cdot\boldsymbol{q}, z_h)_E - \langle(\boldsymbol{u}-\boldsymbol{u}_h)\cdot\boldsymbol{n}c, z_h\rangle_{\partial E}\\ &\quad -\langle \boldsymbol{u}_h\widehat{(\pi_k c} - c)\cdot\boldsymbol{n}, z_h\rangle_{\partial E} + (\boldsymbol{u}_h(\Pi_W c - c), \nabla z_h)_E + ((\boldsymbol{u}-\boldsymbol{u}_h)c, \nabla z_h)_E. \quad (45)\end{aligned}$$

Proof Fix $z_h \in \mathbb{P}_k^{\perp}(E)$. Testing (37c) with $\widehat{w}_h = z_h|_e$, for all $e \subset \partial E$, and summing over all faces e, we have

$$\langle \sigma(\Pi_W c - c), z_h\rangle_{\partial E} = \langle(\boldsymbol{q} - \Pi_{\boldsymbol{V}}\boldsymbol{q})\cdot\boldsymbol{n}, z_h\rangle_{\partial E} - \langle(\boldsymbol{u}_h\widehat{\pi_k c} - \boldsymbol{u}c)\cdot\boldsymbol{n}, z_h\rangle_{\partial E}.$$

Integrating the first term on the right hand side by parts yields

$$\begin{aligned}\langle \sigma(\Pi_W c - c), z_h\rangle_{\partial E} &= (\nabla\cdot(\boldsymbol{q} - \Pi_{\boldsymbol{V}}\boldsymbol{q}), z_h)_E + (\boldsymbol{q} - \Pi_{\boldsymbol{V}}\boldsymbol{q}, \nabla z_h)_E\\ &\quad -\langle(\boldsymbol{u}_h\widehat{\pi_k c} - \boldsymbol{u}c)\cdot\boldsymbol{n}, z_h\rangle_{\partial E}.\end{aligned}$$

Since $\nabla\cdot(\Pi_{\boldsymbol{V}}\boldsymbol{q}) \in \mathbb{P}_{k-1}(E)$ and $z_h \in \mathbb{P}_k^{\perp}(E)$,

$$\langle \sigma(\Pi_W c - c), z_h\rangle_{\partial E} = (\nabla\cdot\boldsymbol{q}, z_h)_E + (\boldsymbol{q} - \Pi_{\boldsymbol{V}}\boldsymbol{q}, \nabla z_h)_E - \langle(\boldsymbol{u}_h\widehat{\pi_k c} - \boldsymbol{u}c)\cdot\boldsymbol{n}, z_h\rangle_{\partial E}.$$

Then, by (37a), we can write this as

$$\langle \sigma(\Pi_W c - c), z_h\rangle_{\partial E} = (\nabla\cdot\boldsymbol{q}, z_h)_E + (\boldsymbol{u}_h\Pi_W c - \boldsymbol{u}c, \nabla z_h)_E - \langle(\boldsymbol{u}_h\widehat{\pi_k c} - \boldsymbol{u}c)\cdot\boldsymbol{n}, z_h\rangle_{\partial E}.$$

The result follows after noting that

$$\begin{aligned}\boldsymbol{u}_h\Pi_W c - \boldsymbol{u}c &= (\boldsymbol{u}_h - \boldsymbol{u})c + \boldsymbol{u}_h(\Pi_W c - c),\\ \boldsymbol{u}_h\widehat{\pi_k c} - \boldsymbol{u}c &= (\boldsymbol{u}_h - \boldsymbol{u})c + \boldsymbol{u}_h(\widehat{\pi_k c} - c).\end{aligned}$$

□

Lemma 8 *Let $k \geq 0$ and suppose $(\boldsymbol{u}, \boldsymbol{q}, c) \in (H^{k+1}(\Omega))^d \cap (H^2(\Omega))^d \times (H^{k+1}(\Omega))^d \times H^{k+1}(\Omega)$. There is a positive constant C independent of h, τ and the functions $c, \boldsymbol{q}, \boldsymbol{u}, \boldsymbol{u}_h$ such that*

$$\begin{aligned}\|\Pi_W c - \pi_k c\|_{L^2(\Omega)} \leq Ch^{k+1}\Big((\sigma_{\max} + \|\boldsymbol{u}\|_{H^2(\Omega)})|c|_{H^{k+1}(\Omega)}\\ + |\nabla\cdot\boldsymbol{q}|_{H^k(\Omega)} + \|c\|_{L^\infty(\Omega)}|\boldsymbol{u}|_{H^{k+1}(\Omega)}\Big), \quad (46)\end{aligned}$$

provided the mesh size satisfies $h \leq h_0$ with h_0 defined by (44). Here,

$$\sigma_{\max} = \|\sigma\|_{L^\infty(\partial\mathcal{E}_h)} \lesssim \|\boldsymbol{u}\|_{H^2(\Omega)} + \max(\|\boldsymbol{D}\|_{L^\infty(\Omega)}, 1).$$

Proof Our starting point is Proposition 1. For brevity, we denote $e_c = \Pi_W c - c$, $\zeta_c = \Pi_W c - \pi_k c$ and $\xi_c = \pi_k c - c$. Observe that $\zeta_c \in P_k^{\perp}(E)$, since (37b) along with the fact that $\mathbb{P}_{k-1}(E) \subset \mathbb{P}_k(E)$ shows that for all $v_h \in \mathbb{P}_{k-1}(E)$,

$$(\Pi_W c - \pi_k c, v_h)_E = (c - \pi_k c, v_h)_E = 0.$$

Testing (45) with $z_h = \zeta_c$, we have

$$\begin{aligned}\langle \sigma(\Pi_W c - c), \zeta_c\rangle_{\partial E} &= (\nabla\cdot \boldsymbol{q}, \zeta_c)_E - \langle (\boldsymbol{u} - \boldsymbol{u}_h)\cdot \boldsymbol{n} c, \zeta_c\rangle_{\partial E}\\ &-\langle \boldsymbol{u}_h(\widehat{\pi_k c} - c)\cdot \boldsymbol{n}, \zeta_c\rangle_{\partial E} + (\boldsymbol{u}_h(\Pi_W c - c), \nabla\zeta_c)_E + ((\boldsymbol{u} - \boldsymbol{u}_h)c, \nabla\zeta_c)_E.\end{aligned}$$

A few algebraic manipulations leads to

$$\begin{aligned}\langle \sigma\zeta_c, \zeta_c\rangle_{\partial E} &= -\langle \sigma\xi_c, \zeta_c\rangle_{\partial E} + (\nabla\cdot \boldsymbol{q}, \zeta_c)_E - \langle (\boldsymbol{u} - \boldsymbol{u}_h)\cdot \boldsymbol{n} c, \zeta_c\rangle_{\partial E}\\ &-\langle \boldsymbol{u}_h(\widehat{\pi_k c} - c)\cdot \boldsymbol{n}, \zeta_c\rangle_{\partial E} + (\boldsymbol{u}_h\zeta_c, \nabla\zeta_c)_E + (\boldsymbol{u}_h\xi_c, \nabla\zeta_c)_E + ((\boldsymbol{u} - \boldsymbol{u}_h)c, \nabla\zeta_c)_E.\end{aligned}$$

Next, noting that $\boldsymbol{u}_h\zeta_c\cdot\nabla\zeta_c = \frac{1}{2}\nabla\cdot(\boldsymbol{u}_h\zeta_c^2) - \frac{1}{2}\zeta_c^2\nabla\cdot\boldsymbol{u}_h$, we apply Gauss's theorem to find

$$(\zeta_c\boldsymbol{u}_h, \nabla\zeta_c)_E = \frac{1}{2}\langle \boldsymbol{u}_h\cdot\boldsymbol{n}\zeta_c, \zeta_c\rangle_{\partial E} - \frac{1}{2}((\nabla\cdot\boldsymbol{u}_h)\zeta_c, \zeta_c)_E, \tag{47}$$

and thus with (43)

$$\begin{aligned}\|\zeta_c\|^2_{L^2(\partial E)} \le &-\langle \sigma\xi_c, \zeta_c\rangle_{\partial E} + (\nabla\cdot\boldsymbol{q}, \zeta_c)_E - \langle (\boldsymbol{u} - \boldsymbol{u}_h)\cdot\boldsymbol{n}c, \zeta_c\rangle_{\partial E}\\ &-\langle \boldsymbol{u}_h(\widehat{\pi_k c} - c)\cdot\boldsymbol{n}, \zeta_c\rangle_{\partial E} + (\boldsymbol{u}_h\xi_c, \nabla\zeta_c)_E + ((\boldsymbol{u} - \boldsymbol{u}_h)c, \nabla\zeta_c)_E\\ &-\frac{1}{2}((\nabla\cdot\boldsymbol{u}_h)\zeta_c, \zeta_c)_E\\ = &\, T_1 + \cdots + T_7.\end{aligned}$$

We now bound each term T_i for $1 \le i \le 7$.

First, by Cauchy–Schwarz's inequality and a discrete trace inequality (see e.g. [14, Lemma 1.46]),

$$\begin{aligned}|T_1| &\le C\|\sigma\|_{L^\infty(\partial\mathcal{E}_h)} h_E^{-1/2}\|\xi_c\|_{L^2(\partial E)}\|\zeta_c\|_{L^2(E)}\\ &\le C\left(\max(\|D\|_{L^\infty(\Omega)}, 1) + \|\boldsymbol{u}_h\|_{L^\infty(\Omega)}\right) h^k|c|_{H^{k+1}(E)}\|\zeta_c\|_{L^2(E)},\end{aligned}$$

by the approximation properties of the L^2-projection π_k. The term T_2 can be bounded by observing that

$$T_2 = (\nabla\cdot\boldsymbol{q}, \zeta_c)_E = (\nabla\cdot\boldsymbol{q} - \pi_{k-1}\nabla\cdot\boldsymbol{q}, \zeta_c)_E,$$

so by the triangle inequality we have

$$|T_2| \le Ch^k|\nabla\cdot\boldsymbol{q}|_{H^k(E)}\|\zeta_c\|_{L^2(E)}.$$

Next, Hölder's inequality, the estimate (26c), and a discrete trace inequality yield

$$\begin{aligned}|T_3| &\le \|c\|_{L^\infty(\Omega)}\left\|(\boldsymbol{u} - \boldsymbol{u}_h)\cdot\boldsymbol{n}\right\|_{L^2(\partial E)}\|\zeta_c\|_{L^2(\partial E)}\\ &\le Ch^k\|c\|_{L^\infty(\Omega)}|\boldsymbol{u}|_{H^{k+1}(E)}\|\zeta_c\|_{L^2(E)}.\end{aligned}$$

As for T_4, we apply Hölder's inequality, to find

$$|T_4| \le \|\boldsymbol{u}_h\cdot\boldsymbol{n}\|_{L^\infty(\partial E)}\|\widehat{\pi_k c} - c\|_{L^2(\partial E)}\|\zeta_c\|_{L^2(\partial E)}.$$

To proceed further, we use the approximation properties of the projection $\widehat{\pi_k c}$ and a discrete trace inequality:

$$|T_4| \le Ch^k\|\boldsymbol{u}_h\|_{L^\infty(\Omega)}|c|_{H^{k+1}(E)}\|\zeta_c\|_{L^2(E)}.$$

Next, by Hölder's inequality, an inverse inequality, and the approximation properties of the projection π_k, we have

$$\begin{aligned}|T_5| &\leq \|\boldsymbol{u}_h\|_{L^\infty(\Omega)}\|\xi_c\|_{L^2(E)}\|\nabla\zeta_c\|_{L^2(E)}\\ &\leq Ch^k\|\boldsymbol{u}_h\|_{L^\infty(\Omega)}|c|_{H^{k+1}(\Omega)}\|\zeta_c\|_{L^2(E)}.\end{aligned}$$

We bound T_6 in a similar fashion, using the error bound (26a):

$$|T_6| \leq Ch^k\|c\|_{L^\infty(\Omega)}|\boldsymbol{u}|_{H^{k+1}(E)}\|\zeta_c\|_{L^2(E)}.$$

Using Lemma 7 and the fact that $\nabla\cdot\boldsymbol{u}_h = \pi_{k-1}f$, we have

$$\begin{aligned}|T_7| &\leq \frac{1}{2}\|\nabla\cdot\boldsymbol{u}_h\|_{L^\infty(\Omega)}\|\zeta_c\|^2_{L^2(E)}\\ &\leq \frac{C_\infty}{2}\|f\|_{L^\infty(\Omega)}\|\zeta_c\|^2_{L^2(E)}.\end{aligned}$$

From Lemma 7, we have

$$\|\zeta_c\|^2_{L^2(E)} \leq C_* h_E\|\zeta_c\|^2_{L^2(\partial E)}.$$

Thus, by combining the above bounds and using Lemma 7, we find there exists a constant $C > 0$, independent of h and τ, such that when $h \leq h_0$, (46) holds. □

To analyze the projection error $\|\boldsymbol{\Pi}_V\boldsymbol{q} - \boldsymbol{q}\|_{L^2(\Omega)}$ we require two auxiliary projections taken from [9, Section 4.3] originally defined in [10]. For a fixed element E, let $e^\star$ be a face of E on which $\sigma|_{\partial E}$ attains its maximum. For any sufficiently regular $\boldsymbol{q}$, we define the projections $\boldsymbol{P}_{V_1}\boldsymbol{q}$ and $\boldsymbol{P}_{V_2}\boldsymbol{q}$ as the elements of $\mathbb{P}_k(E)$ satisfying

$$\forall \boldsymbol{v}_h \in (\mathbb{P}_{k-1}(E))^d, \quad (\boldsymbol{P}_{V_1}\boldsymbol{q}, \boldsymbol{v}_h)_E = (\boldsymbol{q} + \boldsymbol{u}c - \boldsymbol{u}_h\Pi_W c, \boldsymbol{v}_h)_E, \tag{48a}$$

$$\forall e \subset \partial E \setminus e^\star, \quad \forall \widehat{w}_h \in \mathbb{P}_k(e), \quad \langle \boldsymbol{P}_{V_1}\boldsymbol{q}\cdot\boldsymbol{n}, \widehat{w}_h\rangle_e = \langle(\boldsymbol{q} + \boldsymbol{u}c - \boldsymbol{u}_h\widehat{\pi_k c})\cdot\boldsymbol{n}, \widehat{w}_h\rangle_e, \tag{48b}$$

and

$$\forall \boldsymbol{v}_h \in (\mathbb{P}_{k-1}(E))^d, \quad (\boldsymbol{P}_{V_2}\boldsymbol{q}, \boldsymbol{v}_h)_E = (\boldsymbol{q}, \boldsymbol{v}_h)_E, \tag{49a}$$

$$\forall e \subset \partial E \setminus e^\star, \quad \forall \widehat{w}_h \in \mathbb{P}_k(e), \quad \langle \boldsymbol{P}_{V_2}\boldsymbol{q}\cdot\boldsymbol{n}, \widehat{w}_h\rangle_e = \langle\boldsymbol{q}\cdot\boldsymbol{n}, \widehat{w}_h\rangle_e. \tag{49b}$$

That the equations defining $\boldsymbol{P}_{V_1}$ and $\boldsymbol{P}_{V_2}$ are well-posed follows from [10, Lemma 3.1].

Now, fix an element $E \in \mathcal{E}_h$ and observe that the set of unit normals to the faces of E excluding $e^\star$, i.e. $\{\boldsymbol{n}_e \mid e \neq e^\star\}$, forms a basis for $\mathbb{R}^d$. Denote by $\{\widetilde{\boldsymbol{n}}_e \mid e \neq e^\star\}$ the dual basis of $\{\boldsymbol{n}_e \mid e \neq e^\star\}$ satisfying

$$\widetilde{\boldsymbol{n}}_{e_i}\cdot\boldsymbol{n}_{e_j} = \delta_{ij}, \quad e_i, e_j \neq e^\star.$$

We can then write,

$$\forall i = 1, 2, \quad \boldsymbol{q} - \boldsymbol{P}_{V_i}\boldsymbol{q} = \sum_{e\neq e^\star}\big((\boldsymbol{q} - \boldsymbol{P}_{V_i}\boldsymbol{q})\cdot\boldsymbol{n}_e\big)\widetilde{\boldsymbol{n}}_e,$$

Therefore, since

$$\|\boldsymbol{q} - \boldsymbol{P}_{V_i}\boldsymbol{q}\|^2_{L^2(E)} \leq \sum_{e\neq e^\star}\|(\boldsymbol{q} - \boldsymbol{P}_{V_i}\boldsymbol{q})\cdot\boldsymbol{n}_e\|^2_{L^2(E)},$$

it suffices to estimate

$$\|(\boldsymbol{q} - \boldsymbol{P}_{V_i}\boldsymbol{q})\cdot\boldsymbol{n}_e\|_{L^2(E)}, \quad e \neq e^\star.$$

Lemma 9 *Let $k \geq 0$ and suppose $(\boldsymbol{u}, \boldsymbol{q}, c) \in (H^{k+1}(\Omega))^d \cap (H^2(\Omega))^d \times (H^{k+1}(\Omega))^d \times H^{k+1}(\Omega)$. There exists a constant $C > 0$ independent of h such that*

$$\|(\boldsymbol{\Pi}_V \boldsymbol{q} - \boldsymbol{P}_{V_1}\boldsymbol{q}) \cdot \boldsymbol{n}_e\|_{L^2(E)} \leq Ch^{k+1}, \tag{50a}$$

$$\|\boldsymbol{P}_{V_1}\boldsymbol{q} - \boldsymbol{P}_{V_2}\boldsymbol{q}\|_{L^2(E)} \leq Ch^{k+1}, \tag{50b}$$

$$\|(\boldsymbol{P}_{V_2}\boldsymbol{q} - \boldsymbol{q}) \cdot \boldsymbol{n}_e\|_{L^2(E)} \leq Ch^{k+1}. \tag{50c}$$

Proof Note that (50a) follows from the proof of [11, Proposition A.3]. We provide details for completeness. By equations (37a) and (48a) defining $\boldsymbol{\Pi}_V$ and $\boldsymbol{P}_{V_1}$, respectively, we have

$$\begin{aligned}\forall \boldsymbol{v}_h \in (\mathbb{P}_{k-1}(E))^d, \quad &\sum_{e_i \neq e^\star} \sum_{e_j \neq e^\star} ((\boldsymbol{\Pi}_V \boldsymbol{q} - \boldsymbol{P}_{V_1}\boldsymbol{q}) \cdot \boldsymbol{n}_{e_i} \widetilde{\boldsymbol{n}}_{e_i}, \boldsymbol{v}_h \cdot \boldsymbol{n}_{e_j} \widetilde{\boldsymbol{n}}_{e_j})_E \\ &= (\boldsymbol{\Pi}_V \boldsymbol{q} - \boldsymbol{P}_{V_1}\boldsymbol{q}, \boldsymbol{v}_h)_E = 0.\end{aligned}$$

However, since $\tilde{\boldsymbol{n}}_{e_j}$ and $\boldsymbol{n}_{e_j}$ are parallel,

$$\forall \boldsymbol{v}_h \in (\mathbb{P}_{k-1}(E))^d, \quad \sum_{e_i \neq e^\star} ((\boldsymbol{\Pi}_V \boldsymbol{q} - \boldsymbol{P}_{V_1}\boldsymbol{q}) \cdot \boldsymbol{n}_{e_i}, \boldsymbol{v}_h \cdot \widetilde{\boldsymbol{n}}_{e_i})_E = 0.$$

Equivalently, since we can choose e.g. $\boldsymbol{v}_h = w_h \boldsymbol{n}_{e_j}$ for any $w_h \in \mathbb{P}_{k-1}(E)$, we have that

$$\forall w_h \in \mathbb{P}_{k-1}(E), \quad ((\boldsymbol{\Pi}_V \boldsymbol{q} - \boldsymbol{P}_{V_1}\boldsymbol{q}) \cdot \boldsymbol{n}_{e_j}, w_h)_E = 0,$$

and thus $(\boldsymbol{\Pi}_V \boldsymbol{q} - \boldsymbol{P}_{V_1}\boldsymbol{q}) \cdot \boldsymbol{n}_e \in \mathbb{P}_k^\perp(E)$ for each $e \neq e^\star$. For brevity, denote $\zeta_e^{\boldsymbol{q}} = (\boldsymbol{\Pi}_V \boldsymbol{q} - \boldsymbol{P}_{V_1}\boldsymbol{q}) \cdot \boldsymbol{n}_e$.

Next, subtracting (48b) from (37c), we find

$$\forall \widehat{w}_h \in \mathbb{P}_k(e), \quad \forall e \neq e^\star, \quad \langle \zeta_e^{\boldsymbol{q}}, \widehat{w}_h \rangle_e = \langle \sigma(c - \Pi_W c), \widehat{w}_h \rangle_e. \tag{51}$$

By [11, Lemma A.1], the trace map $\gamma_e : P_k^\perp(E) \to \mathbb{P}_k(e)$ is a bijection, so we can choose $\widehat{w}_h$ such that $\widehat{w}_h|_e = \zeta_e^{\boldsymbol{q}}$. Consequently, by the Cauchy–Schwarz's inequality, the triangle inequality, and a discrete trace inequality,

$$\begin{aligned}\|\zeta_e^{\boldsymbol{q}}\|_{L^2(e)} \leq &\sigma_{\max} \|c - \Pi_W c\|_{L^2(e)} \\ \leq &C\sigma_{\max} \left(\|c - \pi_k c\|_{L^2(e)} + h^{-1/2} \|\pi_k c - \Pi_W c\|_{L^2(E)} \right).\end{aligned}$$

Equation (50a) now follows from Lemma 7, Lemma 8, and the approximation properties of the L^2-projection π_k.

Next, we show (50b). By the definition of the projections $\boldsymbol{P}_{V_1}$ and $\boldsymbol{P}_{V_2}$,

$$(\boldsymbol{P}_{V_1}\boldsymbol{q} - \boldsymbol{P}_{V_2}\boldsymbol{q}, \boldsymbol{v}_h)_E = (\boldsymbol{u}c - \boldsymbol{u}_h \Pi_W c, \boldsymbol{v}_h)_E, \quad \forall \boldsymbol{v}_h \in (\mathbb{P}_{k-1}(E))^d, \tag{52a}$$

$$\langle (\boldsymbol{P}_{V_1}\boldsymbol{q} - \boldsymbol{P}_{V_2}\boldsymbol{q}) \cdot \boldsymbol{n}, \widehat{w}_h \rangle_e = \langle \left(\boldsymbol{u}c - \boldsymbol{u}_h \widehat{\Pi}_k c\right) \cdot \boldsymbol{n}, \widehat{w}_h \rangle_e, \quad \forall \widehat{w}_h \in \mathbb{P}_k(e), \tag{52b}$$

for all $e \neq e^\star$. There exists a constant $C > 0$, independent of h, such that

$$\begin{aligned}\|\boldsymbol{P}_{V_1}\boldsymbol{q} - \boldsymbol{P}_{V_2}\boldsymbol{q}\|_{L^2(E)} \leq C\Big(&\|\boldsymbol{u}c - \boldsymbol{u}_h \Pi_W c\|_{L^2(E)} \\ &+ h^{1/2} \sum_{e \neq e^\star} \left\| (\boldsymbol{u}c - \boldsymbol{u}_h \widehat{\pi_k c}) \cdot \boldsymbol{n} \right\|_{L^2(e)} \Big).\end{aligned} \tag{53}$$

To see this, let $\boldsymbol{Z} = \boldsymbol{P}_{V_1}\boldsymbol{q} - \boldsymbol{P}_{V_2}\boldsymbol{q}$, $\boldsymbol{\chi} = \boldsymbol{u}c - \boldsymbol{u}_h \Pi_W c$, and $\omega = (\boldsymbol{u}c - \boldsymbol{u}_h \widehat{\Pi}_k c) \cdot \boldsymbol{n}$ for brevity. Then, we can rewrite (52) as: given $\boldsymbol{\chi} \in L^2(E)$ and $\omega \in L^2(e)$ for all $e \subset \partial E \backslash e^\star$, find $\boldsymbol{Z} \in (\mathbb{P}_k(E))^d$ such that

$$\forall \boldsymbol{v}_h \in (\mathbb{P}_{k-1}(E))^d, \quad (\boldsymbol{Z}, \boldsymbol{v}_h)_E = (\boldsymbol{\chi}, \boldsymbol{v}_h)_E, \tag{54a}$$

$$\forall \widehat{w}_h \in \mathbb{P}_k(e), \quad \langle \boldsymbol{Z}\cdot\boldsymbol{n}, \widehat{w}_h\rangle_e = \langle \omega, \widehat{w}_h\rangle_e. \tag{54b}$$

Equation (53) now follows from the inequality, for a constant C independent of h:

$$\|\boldsymbol{Z}\|_{L^2(E)} \leq C\Big(\|\boldsymbol{\pi}_{k-1}\boldsymbol{Z}\|_{L^2(E)} + h^{1/2}\sum_{e\neq e^\star}\|\boldsymbol{Z}\cdot\boldsymbol{n}\|_{L^2(e)}\Big), \tag{55}$$

which can be derived using a finite dimensional scaling argument with the Piola transformation upon noting that

$$\big\|\widetilde{\boldsymbol{\pi}}_{k-1}\widetilde{\boldsymbol{Z}}\big\|_{L^2(\widetilde{E})} + \sum_{\widetilde{e}\neq\widetilde{e}^\star}\big\|\widetilde{\boldsymbol{Z}}\cdot\widetilde{\boldsymbol{n}}\big\|_{L^2(\widetilde{e})}$$

defines a norm on $(\mathbb{P}_k(\widetilde{E}))^d$, with $\widetilde{E}$ the reference triangle or tetrahedron. Testing (54a) and (54b) with $\boldsymbol{\pi}_{k-1}\boldsymbol{Z}$ and $\boldsymbol{Z}\cdot\boldsymbol{n}$, respectively, we find that

$$\|\boldsymbol{\pi}_{k-1}\boldsymbol{Z}\|_{L^2(E)} \leq \|\boldsymbol{\chi}\|_{L^2(E)}, \quad \|\boldsymbol{Z}\cdot\boldsymbol{n}\|_{L^2(e)} \leq \|\omega\|_{L^2(e)}. \tag{56}$$

Consequently,

$$\begin{aligned}\|\boldsymbol{P}\boldsymbol{v}_1\boldsymbol{q} - \boldsymbol{P}\boldsymbol{v}_2\boldsymbol{q}\|_{L^2(E)} \lesssim \|c(\boldsymbol{u}-\boldsymbol{u}_h)\|_{L^2(E)} + \|\boldsymbol{u}_h(c-\Pi_W c)\|_{L^2(E)}\\ +h^{1/2}\|c\,(\boldsymbol{u}-\boldsymbol{u}_h)\cdot\boldsymbol{n}\|_{L^2(\partial E)} + h^{1/2}\|\boldsymbol{u}_h\cdot\boldsymbol{n}(c-\widehat{\pi_k c})\|_{L^2(\partial E)}.\end{aligned}$$

Equation (50c) now follows from the estimates on the errors $\boldsymbol{u}-\boldsymbol{u}_h$, $c-\Pi_W c$, and $c-\widehat{\pi_k c}$.

Finally, (50c) follows from a standard Bramble–Hilbert style argument as shown in [10, Lemma 3.3]. □

Theorem 2 (HDG projection error) *Let $k \geq 0$ and suppose $(\boldsymbol{u},\boldsymbol{q},c) \in (H^{k+1}(\Omega))^d \cap (H^2(\Omega))^d \times (H^{k+1}(\Omega))^d \times H^{k+1}(\Omega)$. There exists a constant $C>0$ such that*

$$\|c-\Pi_W c\|_{L^2(\Omega)} \leq Ch^{k+1}, \tag{57a}$$

$$\|\boldsymbol{q}-\boldsymbol{\Pi}_{\boldsymbol{V}}\boldsymbol{q}\|_{L^2(\Omega)} \leq Ch^{k+1}, \tag{57b}$$

provided the mesh size satisfies $h < h_0$, with h_0 defined in (44).

4.2.2 The Error Equations

We now derive a set of error equations that will be instrumental in establishing our a priori estimates. The starting point is the following set of equations satisfied by the exact solution, assuming sufficient regularity:

$$(\boldsymbol{D}^{-1}\boldsymbol{q}^n, \boldsymbol{v}_h)_{\mathcal{E}_h} - (c^n, \nabla\cdot\boldsymbol{v}_h)_{\mathcal{E}_h} + \langle c^n, \boldsymbol{v}_h\cdot\boldsymbol{n}\rangle_{\partial\mathcal{E}_h} = 0, \tag{58a}$$

$$(\partial_t c^n, w_h)_{\mathcal{E}_h} - (\boldsymbol{u}c^n + \boldsymbol{q}^n, \nabla w_h)_{\mathcal{E}_h} + \langle \widehat{\boldsymbol{S}}^n\cdot\boldsymbol{n}, w_h\rangle_{\partial\mathcal{E}_h} = (g^n, w_h)_{\mathcal{E}_h}, \tag{58b}$$

$$\langle \widehat{\boldsymbol{S}}^n\cdot\boldsymbol{n}, \widehat{w}_h\rangle_{\partial\mathcal{E}_h} = 0, \tag{58c}$$

for all $(\boldsymbol{v}_h, w_h, \widehat{w}_h) \in \boldsymbol{V}_h \times W_h \times M_h$. Here, we define the exact flux

$$\widehat{\boldsymbol{S}}^n = \boldsymbol{q}^n + \boldsymbol{u}c^n. \tag{59}$$

For brevity, we will denote the errors as:

$$\boldsymbol{e}_{\boldsymbol{q}}^n = \boldsymbol{q}^n - \boldsymbol{q}_h^n, \quad e_c^n = c^n - c_h^n, \quad \widehat{e}_c^n = c^n - \widehat{c}_h^n, \tag{60}$$

the projections of the errors as:

$$\boldsymbol{\zeta}_{\boldsymbol{q}}^n = \Pi_{\boldsymbol{V}}\boldsymbol{q}^n - \boldsymbol{q}_h^n, \quad \zeta_c^n = \Pi_W c^n - c_h^n, \quad \widehat{\zeta}_c^n = \widehat{\pi_k c^n} - \widehat{c}_h^n, \tag{61}$$

and the approximation errors of the projections as:

$$\boldsymbol{\xi}_{\boldsymbol{q}}^n = \boldsymbol{q}^n - \Pi_{\boldsymbol{V}}\boldsymbol{q}^n, \quad \xi_c^n = c^n - \Pi_W c^n, \quad \widehat{\xi}_c^n = c^n - \widehat{\pi_k c^n}. \tag{62}$$

Lemma 10 (The concentration error equations) *Let* $(\boldsymbol{u}, \boldsymbol{q}, c)$ *be sufficiently regular solutions to the Darcy and transport problems,* (1) *and* (3)*, respectively. It holds that*

$$(\boldsymbol{D}^{-1}\boldsymbol{\zeta}_{\boldsymbol{q}}^n, \boldsymbol{v}_h)_{\mathcal{E}_h} - (\zeta_c^n, \nabla\cdot\boldsymbol{v}_h)_{\mathcal{E}_h} + \langle\widehat{\zeta}_c^n, \boldsymbol{v}_h\cdot\boldsymbol{n}\rangle_{\partial\mathcal{E}_h} = -(\boldsymbol{D}^{-1}\boldsymbol{\xi}_{\boldsymbol{q}}^n, \boldsymbol{v}_h)_{\mathcal{E}_h}, \tag{63a}$$

$$\begin{aligned}&(\partial_t c^n - \delta_\tau c_h^n, w_h)_{\mathcal{E}_h} - (\boldsymbol{\zeta}_{\boldsymbol{q}}^n + \boldsymbol{u}_h\zeta_c^n, \nabla w_h)_{\mathcal{E}_h}\\ &\quad + \langle\boldsymbol{\zeta}_{\boldsymbol{q}}^n\cdot\boldsymbol{n} + \boldsymbol{u}_h\cdot\boldsymbol{n}\widehat{\zeta}_c^n + \sigma(\zeta_c^n - \widehat{\zeta}_c^n), w_h\rangle_{\partial\mathcal{E}_h} = 0,\end{aligned} \tag{63b}$$

$$\langle\boldsymbol{\zeta}_{\boldsymbol{q}}^n\cdot\boldsymbol{n} + \boldsymbol{u}_h\cdot\boldsymbol{n}\widehat{\zeta}_c^n + \sigma(\zeta_c^n - \widehat{\zeta}_c^n), \widehat{w}_h\rangle_{\partial\mathcal{E}_h} = 0, \tag{63c}$$

for all $(\boldsymbol{v}_h, w_h, \widehat{w}_h) \in \boldsymbol{V}_h \times W_h \times M_h$.

Proof We begin by noting that, by the second equation defining the HDG projection, (37b) and the definition of the L^2 projection $\widehat{\pi}_k$, we can write (58a) as

$$\forall\boldsymbol{v}_h \in \boldsymbol{V}_h, \quad (\boldsymbol{D}^{-1}\boldsymbol{q}^n, \boldsymbol{v}_h)_{\mathcal{E}_h} - (\Pi_W c^n, \nabla\cdot\boldsymbol{v}_h)_{\mathcal{E}_h} + \langle\widehat{\pi_k c^n}, \boldsymbol{v}_h\cdot\boldsymbol{n}\rangle_{\partial\mathcal{E}_h} = 0.$$

and therefore for any $\boldsymbol{v}_h$ in $\boldsymbol{V}_h$, we obtain

$$(\boldsymbol{D}^{-1}\boldsymbol{\Pi}_{\boldsymbol{V}}\boldsymbol{q}^n, \boldsymbol{v}_h)_{\mathcal{E}_h} - (\Pi_W c, \nabla\cdot\boldsymbol{v}_h)_{\mathcal{E}_h} + \langle\widehat{\pi_k c}, \boldsymbol{v}_h\cdot\boldsymbol{n}\rangle_{\partial\mathcal{E}_h} = -(\boldsymbol{D}^{-1}\xi_{\boldsymbol{q}}^n, \boldsymbol{v}_h)_{\mathcal{E}_h}. \tag{64}$$

Subtracting (11a) from (64), we have

$$\forall\boldsymbol{v}_h \in \boldsymbol{V}_h, \quad (\boldsymbol{D}^{-1}\boldsymbol{\zeta}_{\boldsymbol{q}}^n, \boldsymbol{v}_h)_{\mathcal{E}_h} - (\zeta_c^n, \nabla\cdot\boldsymbol{v}_h)_{\mathcal{E}_h} + \langle\widehat{\zeta}_c^n, \boldsymbol{v}_h\cdot\boldsymbol{n}\rangle_{\partial\mathcal{E}_h} = -(\boldsymbol{D}^{-1}\boldsymbol{\xi}_{\boldsymbol{q}}^n, \boldsymbol{v}_h)_{\mathcal{E}_h},$$

which is precisely (63a).

Next, we derive (63b). Applying the definition of the HDG projection in (58b), we have for all $w_h \in W_h$,

$$\begin{aligned}&(\partial_t c^n, w_h)_{\mathcal{E}_h} - (\boldsymbol{u}_h\Pi_W c^n + \boldsymbol{\Pi}_{\boldsymbol{V}}\boldsymbol{q}^n, \nabla w_h)_{\mathcal{E}_h}\\ &\quad + \langle\boldsymbol{\Pi}_{\boldsymbol{V}}\boldsymbol{q}\cdot\boldsymbol{n} + \boldsymbol{u}_h\cdot\boldsymbol{n}\widehat{\pi_k c} + \sigma(\Pi_W c - c), w_h\rangle_{\partial\mathcal{E}_h} = (g^n, w_h)_{\mathcal{E}_h}.\end{aligned} \tag{65}$$

Subtracting (11b) from (65), we have for all $w_h \in W_h$:

$$\begin{aligned}&(\partial_t c^n - \delta_\tau c_h^n, w_h)_{\mathcal{E}_h} - (\boldsymbol{u}_h\zeta_c^n + \boldsymbol{\zeta}_{\boldsymbol{q}}^n, \nabla w_h)_{\mathcal{E}_h}\\ &\quad + \langle\boldsymbol{\zeta}_{\boldsymbol{q}}^n\cdot\boldsymbol{n} + \boldsymbol{u}_h\cdot\boldsymbol{n}\widehat{\zeta}_c^n + \sigma(\zeta_c^n - \widehat{\zeta}_c^n), w_h\rangle_{\partial\mathcal{E}_h} = 0.\end{aligned}$$

Finally, we turn to (63c). To begin, we use the definition of the HDG projection in (58c) to find:

$$\forall\widehat{w}_h \in M_h, \quad \langle\boldsymbol{\Pi}_{\boldsymbol{V}}\boldsymbol{q}\cdot\boldsymbol{n} + \boldsymbol{u}_h\cdot\boldsymbol{n}\widehat{\pi_k c} + \sigma(\Pi_W c - c), \widehat{w}_h\rangle_{\partial\mathcal{E}_h} = 0. \tag{66}$$

Subtracting (11c) from (66):

$$\forall\widehat{w}_h \in M_h, \quad \langle\boldsymbol{\zeta}_{\boldsymbol{q}}^n\cdot\boldsymbol{n} + \boldsymbol{u}_h\cdot\boldsymbol{n}\widehat{\zeta}_c^n + \sigma(\zeta_c^n - \widehat{\zeta}_c^n), \widehat{w}_h\rangle_{\partial\mathcal{E}_h} = 0,$$

which is (63c). □

Lemma 11 *Assuming $\tau \le 1/C_f$, and $h < h_0$, with h_0 defined in (44), we have*

$$\begin{aligned}&\left\|\zeta_c^m\right\|_{L^2(\Omega)}^2+\tau\sum_{n=1}^m\left\|\boldsymbol{D}^{-1/2}\boldsymbol{\zeta}_{\boldsymbol{q}}^n\right\|_{L^2(\Omega)}^2+2\tau\sum_{n=1}^m\left\|\zeta_c^n-\widehat{\zeta}_c^n\right\|_{L^2(\partial\mathcal{E}_h)}^2\\&\quad\le C\exp(C_fT)\left(h^{2k+2}+\tau^2\right),\end{aligned}\tag{67}$$

where $C_f = 1 + 2C_\infty\left\|f\right\|_{L^\infty(\Omega)}$ and C is a positive constant independent of h and τ.

Proof Testing (63a), (63b), and (63c) with $(\boldsymbol{v}_h, w_h, \widehat{w}_h) = (\boldsymbol{\zeta}_{\boldsymbol{q}}^n, \zeta_c^n, -\widehat{\zeta}_c^n)$, we have:

$$(\boldsymbol{D}^{-1}\boldsymbol{\zeta}_{\boldsymbol{q}}^n,\boldsymbol{\zeta}_{\boldsymbol{q}}^n)_{\mathcal{E}_h}-(\zeta_c^n,\nabla\cdot\boldsymbol{\zeta}_{\boldsymbol{q}}^n)_{\mathcal{E}_h}+\langle\widehat{\zeta}_c^n,\boldsymbol{\zeta}_{\boldsymbol{q}}^n\cdot\boldsymbol{n}\rangle_{\partial\mathcal{E}_h}=-(\boldsymbol{D}^{-1}\boldsymbol{\xi}_{\boldsymbol{q}}^n,\boldsymbol{\zeta}_{\boldsymbol{q}}^n)_{\mathcal{E}_h},\tag{68a}$$

$$\begin{aligned}&(\partial_tc^n-\delta_\tau c_h^n,\zeta_c^n)_{\mathcal{E}_h}-(\boldsymbol{\zeta}_{\boldsymbol{q}}^n+\boldsymbol{u}_h\zeta_c^n,\nabla\zeta_c^n)_{\mathcal{E}_h}\\&\quad+\langle\boldsymbol{\zeta}_{\boldsymbol{q}}^n\cdot\boldsymbol{n}+\boldsymbol{u}_h\cdot\boldsymbol{n}\widehat{\zeta}_c^n+\sigma(\zeta_c^n-\widehat{\zeta}_c^n),\zeta_c^n\rangle_{\partial\mathcal{E}_h}=0,\end{aligned}\tag{68b}$$

$$-\langle\boldsymbol{\zeta}_{\boldsymbol{q}}^n\cdot\boldsymbol{n}+\boldsymbol{u}_h\cdot\boldsymbol{n}\widehat{\zeta}_c^n+\sigma(\zeta_c^n-\widehat{\zeta}_c^n),\widehat{\zeta}_c^n\rangle_{\partial\mathcal{E}_h}=0.\tag{68c}$$

Integrating by parts in (68a), we obtain

$$(\boldsymbol{D}^{-1}\boldsymbol{\zeta}_{\boldsymbol{q}}^n,\boldsymbol{\zeta}_{\boldsymbol{q}}^n)_{\mathcal{E}_h}+(\nabla\zeta_c^n,\boldsymbol{\zeta}_{\boldsymbol{q}}^n)_{\mathcal{E}_h}-\langle\zeta_c^n-\widehat{\zeta}_c^n,\boldsymbol{\zeta}_{\boldsymbol{q}}^n\cdot\boldsymbol{n}\rangle_{\partial\mathcal{E}_h}=-(\boldsymbol{D}^{-1}\boldsymbol{\xi}_{\boldsymbol{q}}^n,\boldsymbol{\zeta}_{\boldsymbol{q}}^n)_{\mathcal{E}_h}.\tag{69}$$

Summing (68b), (68c) and (69), we are left with

$$\begin{aligned}&(\boldsymbol{D}^{-1}\boldsymbol{\zeta}_{\boldsymbol{q}}^n,\boldsymbol{\zeta}_{\boldsymbol{q}}^n)_{\mathcal{E}_h}+(\partial_tc^n-\delta_\tau c_h^n,\zeta_c^n)_{\mathcal{E}_h}-(\boldsymbol{u}_h\zeta_c^n,\nabla\zeta_c^n)_{\mathcal{E}_h}+\\&\langle\boldsymbol{u}_h\cdot\boldsymbol{n}\widehat{\zeta}_c^n,\zeta_c^n-\widehat{\zeta}_c^n\rangle_{\partial\mathcal{E}_h}+\langle\sigma(\zeta_c^n-\widehat{\zeta}_c^n),\zeta_c^n-\widehat{\zeta}_c^n\rangle_{\partial\mathcal{E}_h}=-(\boldsymbol{D}^{-1}\boldsymbol{\xi}_{\boldsymbol{q}}^n,\boldsymbol{\zeta}_{\boldsymbol{q}}^n)_{\mathcal{E}_h}.\end{aligned}$$

Noting that $\boldsymbol{u}_h\zeta_c\cdot\nabla\zeta_c=\frac{1}{2}\nabla\cdot(\boldsymbol{u}_h\zeta_c^2)-\frac{1}{2}\zeta_c^2\nabla\cdot\boldsymbol{u}_h$, we apply Gauss's theorem to find

$$(\boldsymbol{u}_h\zeta_c^n,\nabla\zeta_c^n)_E=\frac{1}{2}\langle\boldsymbol{u}_h\cdot\boldsymbol{n}\zeta_c^n,\zeta_c^n\rangle_{\partial E}-\frac{1}{2}((\nabla\cdot\boldsymbol{u}_h)\zeta_c^n,\zeta_c^n)_E,$$

and therefore, we have

$$\begin{aligned}&(\boldsymbol{D}^{-1}\boldsymbol{\zeta}_{\boldsymbol{q}}^n,\boldsymbol{\zeta}_{\boldsymbol{q}}^n)_{\mathcal{E}_h}+(\partial_tc^n-\delta_\tau c_h^n,\zeta_c^n)_{\mathcal{E}_h}+\frac{1}{2}((\nabla\cdot\boldsymbol{u}_h)\zeta_c^n,\zeta_c^n)_{\mathcal{E}_h}\\&+\langle(\sigma-\frac{1}{2}\boldsymbol{u}_h\cdot\boldsymbol{n})(\zeta_c^n-\widehat{\zeta}_c^n),\zeta_c^n-\widehat{\zeta}_c^n\rangle_{\partial\mathcal{E}_h}=-(\boldsymbol{D}^{-1}\boldsymbol{\xi}_{\boldsymbol{q}}^n,\boldsymbol{\zeta}_{\boldsymbol{q}}^n)_{\mathcal{E}_h}.\end{aligned}\tag{70}$$

Noting that we can write

$$\begin{aligned}\partial_tc^n-\delta_\tau c_h^n&=(\partial_tc^n-\delta_\tau c^n)+\delta_\tau(c^n-c_h^n)\\&=(\partial_tc^n-\delta_\tau c^n)+\delta_\tau\zeta_c^n+\delta_\tau\xi_c^n,\end{aligned}$$

we can multiply (70) by τ and rearrange to find

$$\begin{aligned}&2\tau\left\|\boldsymbol{D}^{-1/2}\boldsymbol{\zeta}_{\boldsymbol{q}}^n\right\|_{L^2(\Omega)}^2+2(\zeta_c^n-\zeta_c^{n-1},\zeta_c^n)_{\mathcal{E}_h}+2\tau\langle\zeta_c^n-\widehat{\zeta}_c^n,\zeta_c^n-\widehat{\zeta}_c^n\rangle_{\partial\mathcal{E}_h}\\&\le-2\tau(\boldsymbol{D}^{-1}\boldsymbol{\xi}_{\boldsymbol{q}}^n,\boldsymbol{\zeta}_{\boldsymbol{q}}^n)_{\mathcal{E}_h}-\tau((\nabla\cdot\boldsymbol{u}_h)\zeta_c^n,\zeta_c^n)_{\mathcal{E}_h}-2\tau(\partial_tc^n-\delta_\tau c^n,\zeta_c^n)_{\mathcal{E}_h}\\&\quad-2\tau(\delta_\tau\xi_c^n,\zeta_c^n)_{\mathcal{E}_h},\end{aligned}\tag{71}$$

where we have used that $\sigma-\frac{1}{2}\boldsymbol{u}_h\cdot\boldsymbol{n}\ge 1$ by (43). By the symmetry of $\boldsymbol{D}$, the Cauchy–Schwarz's inequality, and Young's inequality, we have

$$2\tau|(\boldsymbol{D}^{-1}\boldsymbol{\xi}_{\boldsymbol{q}}^n,\boldsymbol{\zeta}_{\boldsymbol{q}}^n)_{\mathcal{E}_h}|\le\tau\left\|\boldsymbol{D}^{-1/2}\boldsymbol{\xi}_{\boldsymbol{q}}^n\right\|_{L^2(\Omega)}^2+\tau\left\|\boldsymbol{D}^{-1/2}\boldsymbol{\zeta}_{\boldsymbol{q}}^n\right\|_{L^2(\Omega)}^2.$$

Next, we have by Hölder's inequality,

$$\tau|((\nabla\cdot\boldsymbol{u}_h)\zeta_c^n,\zeta_c^n)_{\mathcal{E}_h}|\le C_\infty\tau\|f\|_{L^\infty(\Omega)}\|\zeta_c^n\|_{L^2(\Omega)}^2.$$

Once again, by the Cauchy–Schwarz's inequality and Young's inequality, we have

$$2\tau|(\partial_t c^n-\delta_\tau c^n,\zeta_c^n)_{\mathcal{E}_h}|\le 4\tau\|\partial_t c^n-\delta_\tau c^n\|_{L^2(\Omega)}^2+\frac{\tau}{4}\|\zeta_c^n\|_{L^2(\Omega)}^2.$$

Similarly,

$$2\tau|(\delta_\tau\xi_c^n,\zeta_c^n)_{\mathcal{E}_h}|\le 4\tau\|\delta_\tau\xi_c^n\|_{L^2(\Omega)}^2+\frac{\tau}{4}\|\zeta_c^n\|_{L^2(\Omega)}^2.$$

Collecting the above bounds and using that $2x(x-y)\ge x^2-y^2$, we have

$$\begin{aligned}&\|\zeta_c^n\|_{L^2(\Omega)}^2-\|\zeta_c^{n-1}\|_{L^2(\Omega)}^2+\tau\|\boldsymbol{D}^{-1/2}\boldsymbol{\zeta}_{\boldsymbol{q}}^n\|_{L^2(\Omega)}^2+2\tau\|\zeta_c^n-\widehat{\zeta}_c^n\|_{L^2(\partial\mathcal{E}_h)}^2\\&\le\tau\|\boldsymbol{D}^{-1/2}\boldsymbol{\xi}_{\boldsymbol{q}}^n\|_{L^2(\Omega)}^2\\&\quad+4\tau\|\partial_t c^n-\delta_\tau c^n\|_{L^2(\Omega)}^2+4\tau\|\delta_\tau\xi_c^n\|_{L^2(\Omega)}^2+\tau\left(\frac{1}{2}+C_\infty\|f\|_{L^\infty(\Omega)}\right)\|\zeta_c^n\|_{L^2(\Omega)}^2.\end{aligned}$$

Summing from $n=1,\dots,m$, assuming that

$$\tau\le\frac{1}{1+2C_\infty\|f\|_{L^\infty(\Omega)}},\tag{72}$$

multiplying both sides of the inequality by 2 and rearranging, we find

$$\begin{aligned}&\|\zeta_c^m\|_{L^2(\Omega)}^2+2\tau\sum_{n=1}^m\left(\|\boldsymbol{D}^{-1/2}\boldsymbol{\zeta}_{\boldsymbol{q}}^n\|_{L^2(\Omega)}^2+2\|\zeta_c^n-\widehat{\zeta}_c^n\|_{L^2(\partial\mathcal{E}_h)}^2\right)\\&\le 2\|\zeta_c^0\|_{L^2(\Omega)}^2+2\tau\sum_{n=1}^m\left(\|\boldsymbol{D}^{-1/2}\boldsymbol{\xi}_{\boldsymbol{q}}^n\|_{L^2(\Omega)}^2+4\|\partial_t c^n-\delta_\tau c^n\|_{L^2(\Omega)}^2+4\|\delta_\tau\xi_c^n\|_{L^2(\Omega)}^2\right)\\&\quad+\tau\left(1+2C_\infty\|f\|_{L^\infty(\Omega)}\right)\sum_{n=1}^{m-1}\|\zeta_c^n\|_{L^2(\Omega)}^2.\end{aligned}$$

Thus, the application of a discrete Grönwall inequality yields

$$\begin{aligned}&\|\zeta_c^m\|_{L^2(\Omega)}^2+2\tau\sum_{n=1}^m\left(\|\boldsymbol{D}^{-1/2}\boldsymbol{\zeta}_{\boldsymbol{q}}^n\|_{L^2(\Omega)}^2+2\|\zeta_c^n-\widehat{\zeta}_c^n\|_{L^2(\partial\mathcal{E}_h)}^2\right)\\&\le 2\exp\left(C_f T\right)\|\zeta_c^0\|_{L^2(\Omega)}^2\\&\quad+2\exp\left(C_f T\right)\tau\sum_{n=1}^m\left(\|\boldsymbol{D}^{-1/2}\boldsymbol{\xi}_{\boldsymbol{q}}^n\|_{L^2(\Omega)}^2+4\|\partial_t c^n-\delta_\tau c^n\|_{L^2(\Omega)}^2+4\|\delta_\tau\xi_c^n\|_{L^2(\Omega)}^2\right),\end{aligned}$$

where $C_f=1+2C_\infty\|f\|_{L^\infty(\Omega)}$.

Using (57b), we have:

$$\tau\sum_{n=1}^m\|\boldsymbol{D}^{-1/2}\boldsymbol{\xi}_{\boldsymbol{q}}^n\|_{L^2(\Omega)}^2\le CTh^{2k+2}.$$

Similarly, using (57a), we have

$$\tau \sum_{n=1}^{m} \|\delta_\tau \xi_c^n\|^2_{L^2(\Omega)} = \tau \sum_{n=1}^{m} \|\delta_\tau c^n - \Pi_W(\delta_\tau c^n)\|^2_{L^2(\Omega)} \leq CTh^{2k+2}.$$

Next, Taylor's theorem yields:

$$\tau \sum_{n=1}^{m} \|\partial_t c^n - \delta_\tau c^n\|^2_{L^2(\Omega)} \leq C\tau^2 \int_0^{t_m} \|\partial_{tt} c\|^2_{L^2(\Omega)}.$$

Finally, since we initialize the numerical method with $c_h^0 = \pi_k c_0$, by Lemma 8 we have:

$$\left\|\zeta_c^0\right\|^2_{L^2(\Omega)} \leq Ch^{2k+2}.$$

Collecting the above bounds, we obtain the desired result (67). □

Theorem 3 (Error estimate) *Let $k \geq 0$ and suppose $(\boldsymbol{u}, \boldsymbol{q}, c) \in (H^{k+1}(\Omega))^d \cap (H^2(\Omega))^d \times (H^{k+1}(\Omega))^d \times H^{k+1}(\Omega)$ are solutions to the Darcy and transport problems, (1) and (3), respectively. Assuming $\tau \leq 1/C_f$, and $h < h_0$, with h_0 defined in (44), we have*

$$\left\|c^m - c_h^m\right\|^2_{L^2(\Omega)} + \tau \sum_{n=1}^{m} \left\|\boldsymbol{D}^{-1/2}(\boldsymbol{q}^n - \boldsymbol{q}_h^n)\right\|^2_{L^2(\Omega)} \leq C \exp(C_f T)\left(h^{2k+2} + \tau^2\right),$$

$$\tau \sum_{n=1}^{m} \left\|c^n - \widehat{c}_h^n\right\|^2_{L^2(\partial\mathcal{E}_h)} \leq C \exp(C_f T)\left(h^{2k+1} + \tau^2\right),$$

where $C_f = 1 + 2C_\infty \left\|f\right\|_{L^\infty(\Omega)}$ and C is a positive constant independent of h and τ.

Proof Follows from the triangle inequality, Lemma 11, the approximation properties of Π_W, $\boldsymbol{\Pi}_V$, $\widehat{\pi}_k$, and the fact that $\exp(C_f T) \geq 1$. □

5 Numerical Results

In this section, we perform three numerical experiments to test our algorithm and compare with our theoretical results. All simulations have been implemented using Netgen/NGSolve [26, 27]. In each case, we employ static condensation for both the flow and transport problems to eliminate the interior degrees of freedom (dofs) resulting in a reduction in the size of the global systems. We briefly review this key feature of hybrid mixed methods and hybridizable discontinuous Galerkin methods below. While our discussion will center around the hybridizable discontinuous Galerkin method for the transport problem, similar considerations hold for the hybrid mixed method for the flow problem.

As outlined in [25], at each time step we can express the transport problem (11a)–(11c) in matrix form:

$$\begin{bmatrix} \boldsymbol{A} & -\boldsymbol{B}^T & \boldsymbol{D}^T \\ \boldsymbol{B} & \boldsymbol{E} & \boldsymbol{G} \\ \boldsymbol{D} & \boldsymbol{H} & \boldsymbol{J} \end{bmatrix} \begin{bmatrix} \boldsymbol{Q} \\ \boldsymbol{C} \\ \widehat{\boldsymbol{C}} \end{bmatrix} = \begin{bmatrix} \boldsymbol{0} \\ \boldsymbol{F} \\ \boldsymbol{0} \end{bmatrix}, \tag{73}$$

whence we can obtain the following statically condensed system for $\widehat{\boldsymbol{C}}$ by eliminating both $\boldsymbol{Q}$ and $\boldsymbol{C}$ locally on each element:

$$\mathbb{K}\widehat{\boldsymbol{C}} = \mathbb{F}, \tag{74}$$

where the matrices $\mathbb{K}$ and $\mathbb{F}$ are defined as

$$\mathbb{K} = \boldsymbol{J} - \begin{bmatrix} \boldsymbol{D} & \boldsymbol{H} \end{bmatrix} \begin{bmatrix} \boldsymbol{A} & -\boldsymbol{B}^T \\ \boldsymbol{B} & \boldsymbol{D} \end{bmatrix}^{-1} \begin{bmatrix} \boldsymbol{D}^T \\ \boldsymbol{G} \end{bmatrix}, \tag{75}$$

$$\mathbb{F} = -\begin{bmatrix} \boldsymbol{D} & \boldsymbol{H} \end{bmatrix} \begin{bmatrix} \boldsymbol{A} & -\boldsymbol{B}^T \\ \boldsymbol{B} & \boldsymbol{D} \end{bmatrix}^{-1} \begin{bmatrix} \boldsymbol{0} \\ \boldsymbol{F} \end{bmatrix}. \tag{76}$$

Once $\widehat{\boldsymbol{C}}$ has been computed, $\boldsymbol{Q}$ and $\boldsymbol{C}$ can be obtained using the fact that

$$\begin{bmatrix} \boldsymbol{Q} \\ \boldsymbol{C} \end{bmatrix} = \begin{bmatrix} \boldsymbol{A} & -\boldsymbol{B}^T \\ \boldsymbol{B} & \boldsymbol{D} \end{bmatrix}^{-1} \left(\begin{bmatrix} \boldsymbol{0} \\ \boldsymbol{F} \end{bmatrix} - \begin{bmatrix} \boldsymbol{D}^T \\ \boldsymbol{G} \end{bmatrix} \widehat{\boldsymbol{C}} \right), \tag{77}$$

and this calculation can be performed in an element-by-element fashion. Consequently, the only globally coupled degrees of freedom arising from the system (11a)–(11c) that remain after static condensation are those associated with $\widehat{\boldsymbol{C}}$, the concentration on the mesh skeleton. As these degrees of freedom are defined solely on $(d-1)$-dimensional facets, the resulting statically condensed system enjoys a global system of size $\mathcal{O}(k^{d-1})$ in comparison to $\mathcal{O}(k^d)$ for classical discontinuous Galerkin methods.

5.1 Manufactured Solution

To verify the theoretical rates of convergence predicted by Theorem 3, we use the method of manufactured solutions on the unit square $\Omega = [0,1]^2$. The source term and boundary condition for the Darcy problem (1) are chosen such that the exact solution is given by

$$\boldsymbol{u}(x,y) = \begin{bmatrix} -2\pi \sin(\pi x) \exp(\frac{y}{2}) \\ 1/\pi \cos(\pi x) \exp(\frac{y}{2}) \end{bmatrix}, \quad p(x,y) = -\frac{2}{\pi} \cos(\pi x) \exp(\tfrac{y}{2}), \tag{78}$$

and the source term and boundary condition for the transport problem (3) are chosen such that the exact solution is given by

$$c(x,y,t) = \sin(2\pi(x-t)) \cos(2\pi(y-t)). \tag{79}$$

For simplicity, the conductivity and diffusion matrices are the identity matrix. First we compute the discrete Darcy velocity using the hybrid mixed method (10) and then apply the HDG scheme (11) with $k = 1, 2, 3$ for a sequence of mesh and time step sizes $h_j = 1/2^j$ and $\tau_j = 1/2^{(k+1)j}$ until the end time $T = 0.1$. The errors for the pressure, the post-processed pressure, and velocity are shown in Table 1; optimal rates are obtained, as expected from Theorem 1. See Remark 1 for details on the post-processing.

Table 2 displays the errors for the concentration and its gradient in the L^2 norm at the final time, as well as in the following norm

$$\left\| \boldsymbol{e}_q \right\|_{\ell^2(L^2,\boldsymbol{D})} = \left(\tau \sum_{n=1}^{N} \left\| \boldsymbol{D}^{-1/2} (\boldsymbol{q}^n - \boldsymbol{q}_h^n) \right\|_{L^2(\Omega)}^2 \right)^{1/2}. \tag{80}$$

Examining the results in Table 2, the estimated order of convergence in the L^2-norm appears to approach $k+1$ for both the scalar and flux variables, as well as in the $\ell^2(L^2)$ norm for the flux variable, in full agreement with the prediction of Theorem 3.

We consider a convection dominated problem wherein a contaminant is transported along a channel at a constant velocity. We wish to evaluate the accuracy of the solution obtained with increasing polynomial degree. The domain is $\Omega = [0, 2.5] \times [0, 0.5]$, and for simplicity

Table 1 Errors in the pressure and velocity between the exact solutions p, $\boldsymbol{u}$ and the discrete solutions p_h, $\boldsymbol{u}_h$, and post-processed pressure $p_h^\star$ computed in the L^2-norm

	h_j	$\|p - p_h\|_{L^2(\Omega)}$	Rate	$\|\boldsymbol{u} - \boldsymbol{u}_h\|_{L^2(\Omega)}$	Rate	$\|p - p_h^\star\|_{L^2(\Omega)}$	Rate
$k=1$	$1/2$	2.252×10^{-1}	–	3.087×10^{-1}	–	8.205×10^{-2}	–
	$1/2^2$	1.116×10^{-1}	1.013	8.001×10^{-2}	1.948	2.106×10^{-2}	1.962
	$1/2^3$	5.545×10^{-2}	1.009	2.022×10^{-1}	1.985	5.305×10^{-3}	1.989
	$1/2^4$	2.767×10^{-2}	1.003	5.069×10^{-3}	1.996	1.329×10^{-3}	1.997
	$1/2^5$	1.383×10^{-2}	1.000	1.268×10^{-3}	1.999	3.324×10^{-4}	1.999
$k=2$	$1/2$	4.176×10^{-2}	–	3.082×10^{-2}	–	3.640×10^{-3}	–
	$1/2^2$	1.065×10^{-2}	1.971	3.828×10^{-3}	3.009	2.321×10^{-4}	3.971
	$1/2^3$	2.678×10^{-3}	1.992	4.736×10^{-4}	3.015	1.455×10^{-5}	3.996
	$1/2^4$	6.703×10^{-4}	1.998	5.889×10^{-5}	3.008	9.089×10^{-7}	4.000
	$1/2^5$	1.676×10^{-4}	1.999	7.343×10^{-6}	3.004	5.678×10^{-8}	4.001
$k=3$	$1/2$	5.475×10^{-3}	–	2.396×10^{-3}	–	1.997×10^{-4}	–
	$1/2^2$	6.968×10^{-4}	2.974	1.486×10^{-4}	4.011	6.160×10^{-6}	5.019
	$1/2^3$	8.749×10^{-5}	2.993	9.215×10^{-6}	4.011	1.898×10^{-7}	5.020
	$1/2^4$	1.095×10^{-5}	2.998	5.732×10^{-7}	4.007	5.884×10^{-9}	5.011
	$1/2^5$	1.369×10^{-6}	2.998	3.573×10^{-8}	4.004	1.831×10^{-10}	5.006

Table 2 Errors in the concentration and flux between the exact solutions c, $\boldsymbol{q}$ and the discrete solutions c_h, $\boldsymbol{q}_h$ computed in various norms

	h_j	τ_j	$\|e_c^N\|_{L^2(\Omega)}$	Rate	$\|\boldsymbol{e}_{\boldsymbol{q}}^N\|_{L^2(\Omega)}$	Rate	$\|\boldsymbol{e}_{\boldsymbol{q}}\|_{\ell^2(L^2,\boldsymbol{D})}$	Rate
$k=1$	$1/2$	$1/2^2$	2.162×10^{0}	–	2.712×10^{0}	–	1.356×10^{0}	–
	$1/2^2$	$1/2^4$	4.789×10^{-1}	2.174	8.489×10^{-1}	1.676	3.085×10^{-1}	2.136
	$1/2^3$	$1/2^6$	1.361×10^{-1}	1.815	2.187×10^{-1}	1.956	7.913×10^{-2}	1.962
	$1/2^4$	$1/2^8$	3.965×10^{-2}	1.779	5.531×10^{-2}	1.983	2.039×10^{-2}	1.956
	$1/2^5$	$1/2^{10}$	9.608×10^{-3}	2.045	1.387×10^{-2}	1.996	5.221×10^{-3}	1.966
$k=2$	$1/2$	$1/2^3$	4.329×10^{-1}	–	8.805×10^{-1}	–	3.113×10^{-1}	–
	$1/2^2$	$1/2^6$	1.099×10^{-1}	1.976	1.871×10^{-1}	2.235	6.869×10^{-2}	2.180
	$1/2^3$	$1/2^9$	1.606×10^{-2}	2.776	2.402×10^{-2}	2.961	9.363×10^{-3}	2.875
	$1/2^4$	$1/2^{12}$	1.953×10^{-3}	3.039	2.995×10^{-3}	3.004	1.198×10^{-3}	2.966
	$1/2^5$	$1/2^{15}$	2.411×10^{-4}	3.018	3.738×10^{-4}	3.002	1.507×10^{-4}	2.991
$k=3$	$1/2$	$1/2^4$	3.264×10^{-1}	–	3.936×10^{-1}	–	1.536×10^{-1}	–
	$1/2^2$	$1/2^8$	2.011×10^{-2}	4.021	2.260×10^{-2}	4.122	1.239×10^{-2}	3.631
	$1/2^3$	$1/2^{12}$	1.366×10^{-3}	3.880	1.313×10^{-3}	4.105	8.404×10^{-4}	3.883
	$1/2^4$	$1/2^{16}$	8.204×10^{-5}	4.057	7.884×10^{-5}	4.058	5.301×10^{-5}	3.987
	$1/2^5$	$1/2^{20}$	5.063×10^{-6}	4.018	4.854×10^{-6}	4.022	3.313×10^{-6}	4.000

Table 3 Number of mesh elements and number of degrees of freedom used for each simulation

k	1	5	1	6	1	7	1	7
N_h	800	264	2888	800	11464	2888	46516	11464
N_{dofs}	2496	2520	8856	8736	34776	35424	140316	139104

Fig. 1 The channel $\Omega = [0, 2.5] \times [0, 0.5]$ and contaminant plume. Top: The initial plume at $t = 0$. Bottom: The plume at $t = 1$

we take it to be a homogeneous medium with permeability equal to one. We choose the problem data for the flow problem such that the velocity is $\boldsymbol{u}(x, y) = [8/5, 0]^T$. We set the diffusion coefficient to 10^{-6}. Initially, the contaminant is concentrated in a ball of radius $r = 0.05$ centered at the point $(x_0, y_0) = (0.25, 0.25)$; that is,

$$c_0(x, y) = \begin{cases} 1, & B_r(x_0, y_0), \\ 0, & \Omega \setminus B_r(x_0, y_0). \end{cases} \tag{81}$$

We run eight simulations to qualitatively compare the use of linear piecewise polynomials on a sequence of increasingly finer meshes to the use of piecewise polynomials of degree $k = 5, 6, 7$ with a comparable cost. Table 3 displays the number of mesh elements N_h and the number of globally coupled degrees of freedom N_{dofs} for each simulation. Simulations with comparable N_{dofs} are grouped together. The final time is $T = 1$ and we fix the time step to $\tau = 10^{-4}$. Figure 1 displays the concentration contour at $t = 0$ and $t = T$ for the choice of $k = 7$ on a mesh with 2888 elements. We observe that the tracer is transported from left to right, as expected. The physical diffusion is small and the concentration contour at the final time remains sharp, which indicates negligible numerical diffusion.

We now show the numerical concentrations obtained with the different choices of polynomial degrees and mesh size in Fig. 2. We first note that the concentration contour on the coarsest mesh for $k = 1$ exhibits significant numerical diffusion. As the mesh size is refined (top row of Fig. 2), the numerical diffusion becomes negligible and the concentration contour for piecewise linears with 143016 globally coupled degrees of freedom (dofs) appears to converge to a sharp plume. The bottom row of Fig. 2 shows the concentration contours obtained with higher polynomial degrees such that the number of globally coupled degrees of freedom is comparable to the one used for piecewise linears on various meshes. We observe that while the concentration contour on the coarsest mesh (800 elements) for $k = 5$ is more accurate than the one obtained with $k = 1$ (with a comparable cost: 2496 versus 2520 dofs), it still shows some numerical diffusion. This seems to indicate that the number of degrees of freedom is too small to capture the correct solution. The solution obtained with $k = 6$ on a mesh with 800 elements is more accurate than the solution with $k = 1$ with comparable cost. As the polynomial degree increases to $k = 7$ and the mesh is finer, we obtain a converged solution for the concentration that exhibits a sharp contour. Figure 2 shows that it is advantageous to use higher order polynomial approximations on coarser meshes than piecewise linears on finer meshes for this numerical example.

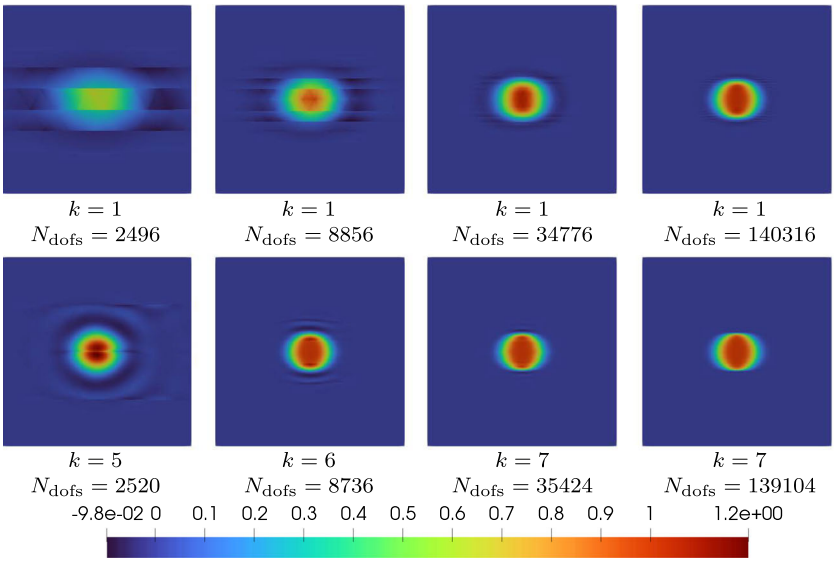

Fig. 2 Close-up snapshots of the concentration plume in the region $[1.6, 2.1] \times [0, 5] \subset \Omega$ at $T = 1$ for various polynomial degrees and mesh sizes

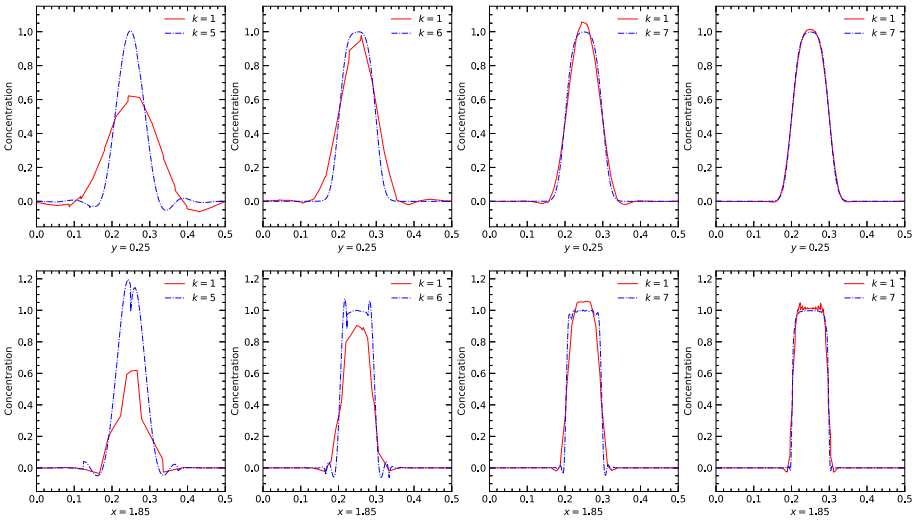

Fig. 3 Profiles of concentration extracted along horizontal line (top row) and vertical line (bottom row), for different polynomial degrees and different mesh sizes

To better compare the numerical solutions, the concentration profiles are extracted along both a horizontal line ($y = 0.25$) and a vertical line ($x = 1.85$) in Fig. 3. Overshoots and undershoots are observed in the neighborhood of the solution front, specially in the profiles along the vertical line. Overall as N_{dofs} (from left to right in each row of Fig. 3), the approximation of the concentration improves. The solution obtained with $k = 1$ with 2496 dofs is more diffuse than the solution obtained with $k = 5$ with comparable cost (2520 dofs); the highest value of the concentration is about 0.6 as opposed to about 1 for $k = 5$.

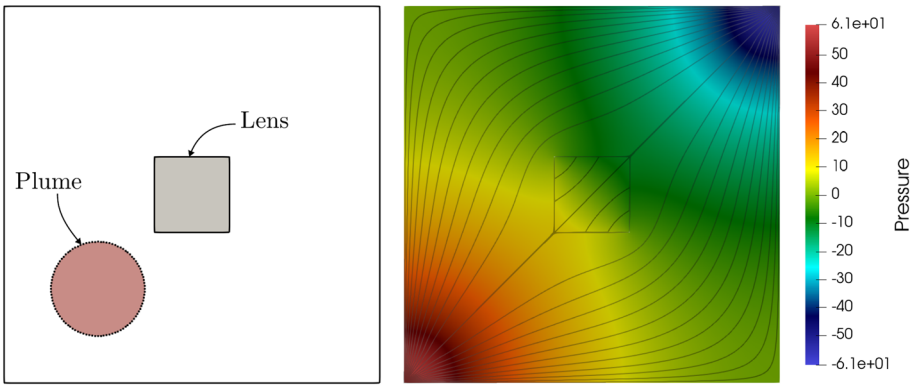

Fig. 4 Left: set-up showing the location of the permeability lens and the initial plume. Right: pressure contours and streamlines

However, the amount of overshoot and undershoot is significant for the solution with $k = 5$. With higher degree $k = 7$, we observe a reduction of the overshoots and undershoots (third figure on each row). As the mesh is further refined (fourth figure on each row), the solution becomes more accurate. The solution with piecewise linears is much closer to the solution obtained with $k = 7$ but there are some small oscillations in the piecewise linear solution in the profile along the vertical line. Figure 3 confirms that the higher order polynomial solutions provide a better approximation of the concentration than the linear polynomial solution with comparable number of dofs. Overshoot and undershoot phenomena are present in the higher order solution but they decrease as the polynomial degree further increases.

5.2 Contaminant Transport in Medium with Permeability Lens

Next, we consider the transport of a contaminant in a porous medium with a permeability lens. The domain is $\Omega = [0, 1]^2$, and the permeability is 9.44×10^{-3} everywhere except for the lens $[0.4, 0.6]^2$ where it is taken to be 9.44×10^{-6}. We split the source term for the flow problem into $f = q^I - q^P$, where q^I and q^P are piecewise constant on $[0.1, 0.1]^2$ and $[0.9, 1]^2$, respectively, and satisfy

$$\int_\Omega q^I \mathrm{d}x = \int_\Omega q^P \mathrm{d}x = 0.36. \tag{82}$$

We impose a no-flow boundary condition $\boldsymbol{u} \cdot \boldsymbol{n}|_{\partial\Omega} = 0$ and a zero-mean condition on the pressure to ensure it is uniquely defined.

Initially, the contaminant is concentrated in a ball of radius $r = 0.125$ centered at the point $(x_0, y_0) = (0.25, 0.25)$, similar to (81). The set-up of the problem is shown in the left panel of Fig. 4: the permeability lens is the gray square, and the initial plume is in pink. Contours of the pressure field are displayed in the right panel of Fig. 4, as well as the streamlines. As expected, the direction of the flow is from the source location to the sink location. While not shown in that figure, the velocity magnitude is much smaller inside the permeability lens. This is made evident in Fig. 5. Snapshots of the concentration contours at $t = 0.75, 1.0, 1.25$ show that the plume is transported along the principal direction of the flow while avoiding the square inclusion. We compare the numerical solutions obtained with different polynomial degrees: $k = 1, 3, 5$, on the same mesh made of 8890 elements,

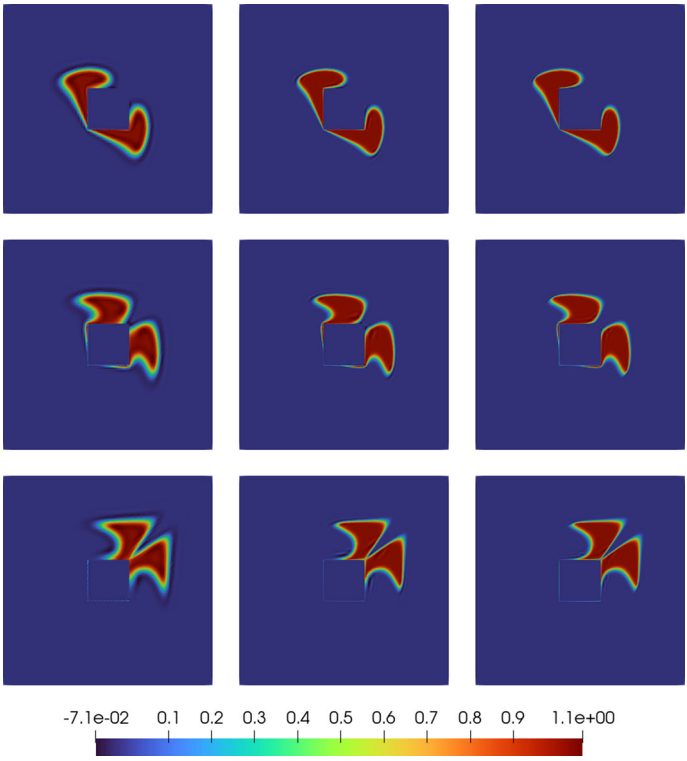

Fig. 5 Snapshots of concentration obtained with different polynomial degrees

which yields 26926, 53852 and 80778 coupled degrees of fredom. The initial circular plume splits itself into two plumes that propagate around the permeability lens and merge again at a later time. We plot the concentration profiles along the line $y = 1.225 - x$ at time $t = 1.25$ in Fig. 6. All three different approximations produce similar profiles with relatively sharp fronts. The solutions obtained with $k = 3$ and $k = 5$ are very close to each other. The piecewise linear approximation shows a more diffusive profile, in particular in the narrow region where the two parts of the plume merge again after the square inclusion. We observe that for all three simulations, the plume does not penetrate the permeability lens. The front in the surrounding rock matrix becomes sharper as the polynomial degree increases.

Finally we comment on the amount of overshoot/undershoot that is being observed in the numerical solution. Throughout the simulations, the magnitude of the overshoot and undershoot is small and remains bounded. Figure 7 displays the concentration contours at $t = 1.0$: elements where there is overshoot or undershoot are colored in white. This figure shows that the number of elements where overshoot and undershoot occurs decreases as the polynomial degree increases. We have also observed that the magnitude of the overshoot or undershoot decreases as the polynomial degree increases from $k = 1$ to $k = 3$, and from $k = 3$ to $k = 5$. Figure 8 displays in green (resp. orange) the elements where the overshoot (resp. undershoot) is above 0.005. The solutions obtained with higher order approximation exhibit reduced overshoot/undershoot both in magnitude and in area.

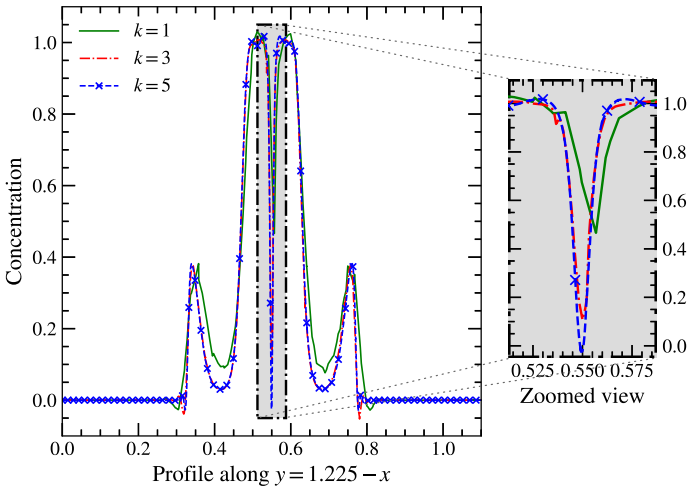

Fig. 6 Concentration profiles along the line $y = 1.225 - x$ at $t = 1.25$ and a close-up view

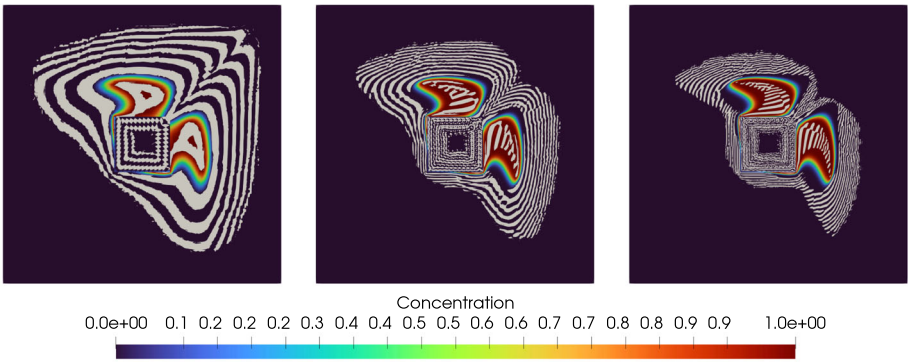

Fig. 7 Concentration contours at $t = 1.0$ for $k = 1$ (left), $k = 3$ (center) and $k = 5$ (right). Elements with overshoot or undershoot are colored in white

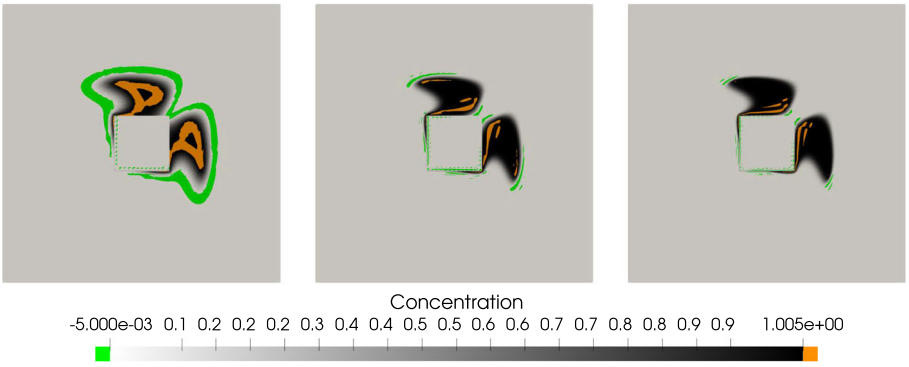

Fig. 8 Concentration contours at $t = 1.0$ for for $k = 1$ (left), $k = 3$ (center) and $k = 5$ (right). Overshoot and undershoot above 0.005 are in green and orange respectively

6 Conclusions

The analysis of the HDG method is obtained for the one-way coupled flow and transport problem. The stabilization term is carefully constructed and depends on the normal component of the velocity as well as the diffusion coefficient. Optimal rates are proved for the scalar and flux variables. The error analysis relies on a modified HDG projection that satisfies optimal bounds. Numerical simulations demonstrate the benefit of using higher order of approximation as opposed to piecewise linears. Solutions obtained with comparable costs exhibit sharper fronts if higher order polynomials are used. Increasing the polynomial degree also has a positive impact in reducing the amount of overshoot and undershoot and the number of elements where these phenomena occur.

Funding Keegan L. A. Kirk gratefully acknowledges support from the Natural Sciences and Engineering Research Council of Canada through the Postdoctoral Fellowship Program (PDF-568008); Beatrice Riviere gratefully acknowledges support from the National Science Foundation NSF-DMS 2111459.

Data Availability The data can be obtained from the authors on reasonable request.

Declarations

Conflict of interest The authors declare that they have no Conflict of interest.

References

1. Arbogast, T., Xiao, H.: Two-level mortar domain decomposition preconditioners for heterogeneous elliptic problems. Comput. Methods Appl. Mech. Eng. **292**, 221–242 (2015). https://doi.org/10.1016/j.cma.2014.10.049
2. Arnold, D.N., Brezzi, F., Cockburn, B., Marini, L.D.: Unified analysis of discontinuous Galerkin methods for elliptic problems. SIAM J. Numer. Anal. (2002). https://doi.org/10.1137/S0036142901384162
3. Boffi, D., Brezzi, F., Fortin, M.: Mixed Finite Element Methods and Applications, Springer Series in Computational Mathematics, vol. 44. Springer (2013)
4. Brezzi, F., Douglas, J., Jr., Durán, R., Fortin, M.: Mixed finite elements for second order elliptic problems in three variables. Numer. Math. **51**, 237–250 (1987)
5. Brezzi, F., Douglas, J., Jr., Marini, L.D.: Two families of mixed elements for second order elliptic problems. Numer. Math. **88**, 217–235 (1985)
6. Cesmelioglu, A., Pham, D., Rhebergen, S.: A hybridizable discontinuous Galerkin method for the fully coupled time-dependent Stokes/Darcy-transport problem. ESAIM: M2AN **57**, 1257–1296 (2023). https://doi.org/10.1051/m2an/2023016
7. Cesmelioglu, A., Rhebergen, S.: A compatible embedded-hybridized discontinuous Galerkin method for the Stokes-Darcy-transport problem. Commun. Appl. Math. Comput. **4**, 293–318 (2021). https://doi.org/10.1007/s42967-020-00115-0
8. Chen, G., Hu, W., Shen, J., Singler, J., Zhang, Y., Zheng, X.: An HDG method for distributed control of convection diffusion PDEs. J. Comput. Appl. Math. **343**, 643–661 (2018). https://doi.org/10.1016/j.cam.2018.05.028
9. Chen, Y., Cockburn, B.: Analysis of variable-degree HDG methods for convection-diffusion equations. Part i: general nonconforming meshes. IMA J. Numer. Anal. **32**(4), 1267–1293 (2012). https://doi.org/10.1093/imanum/drr058
10. Cockburn, B., Dong, B.: An analysis of the minimal dissipation local discontinuous Galerkin method for convection-diffusion problems. J. Sci. Comput. **32**(2), 233–262 (2007). https://doi.org/10.1007/s10915-007-9130-3
11. Cockburn, B., Gopalakrishnan, J., Sayas, F.: A projection-based error analysis of HDG methods. Math. Comput. **79**, 1351–1367 (2010). https://doi.org/10.1090/S0025-5718-10-02334-3
12. Cockburn, B., Guzmán, J., Wang, H.: Superconvergent discontinuous Galerkin methods for second-order elliptic problems. Math. Comput. **78**, 1–24 (2009). https://doi.org/10.1090/S0025-5718-08-02146-7

13. Darlow, B., Ewing, R., Wheeler, M.: Mixed finite flement method for miscible displacement problems in porous media. Soc. Pet. Eng. J. **24**(04), 391–398 (1984). https://doi.org/10.2118/10501-PA
14. Di Pietro, D.A., Ern, A.: Mathematical Aspects of Discontinuous Galerkin Methods, Mathématiques et Applications, vol. 69. Springer-Verlag, Berlin Heidelberg (2012)
15. Douglas, J., Jr., Ewing, R., Wheeler, M.: The approximation of the pressure by a mixed method in the simulation of miscible displacement. RAIRO. Anal. numér. **17**(1), 17–33 (1983). https://doi.org/10.1051/m2an/1983170100171
16. Du, S., Sayas, F.J.: An Invitation to the Theory of the Hybridizable Discontinuous Galerkin Method: Projections, Estimates, Tools. Springer Briefs in Mathematics. Springer International Publishing (2019)
17. Egger, H., Schöberl, J.: A hybrid mixed discontinuous Galerkin finite-element method for convection-diffusion problems. IMA J. Numer. Anal. **30**(4), 1206–1234 (2010). https://doi.org/10.1093/imanum/drn083
18. Ern, A., Guermond, J.L.: Finite Elements I. Texts in Applied Mathematics. Springer International Publishing (2021). https://doi.org/10.1007/978-3-030-56341-7
19. Ewing, R., Russell, T., Wheeler, M.: Convergence analysis of an approximation of miscible displacement in porous media by mixed finite elements and a modified method of characteristics. Comput. Methods Appl. Mech. Eng. **47**(1), 73–92 (1984). https://doi.org/10.1016/0045-7825(84)90048-3
20. Fabien, M., Knepley, M., Riviere, B.: A high order hybridizable discontinuous Galerkin method for incompressible miscible displacement in heterogeneous media. Results Appl. Math. (2020). https://doi.org/10.1016/j.rinam.2019.100089
21. Fu, G., Yang, Y.: A hybrid-mixed finite element method for single-phase Darcy flow in fractured porous media. Adv. Water Resour. (2022). https://doi.org/10.1016/j.advwatres.2022.104129
22. Girault, V., Raviart, P.A.: Finite Element Methods for Navier–Stokes Equations: Theory and Algorithms, vol. 5. Springer-Verlag (1986)
23. Nédélec, J.C.: Mixed finite elements in $\mathbb{R}^3$. Numer. Math. **35**, 315–341 (1980)
24. Nédélec, J.C.: A new family of mixed finite elements in $\mathbb{R}^3$. Numer. Math. **50**, 57–81 (1986)
25. Nguyen, N., Peraire, J., Cockburn, B.: An implicit high-order hybridizable discontinuous Galerkin method for linear convection-diffusion equations. J. Comput. Phys. **228**(9), 3232–3254 (2009). https://doi.org/10.1016/j.jcp.2009.01.030
26. Schöberl, J.: NETGEN—An advancing front 2D/3D-mesh generator based on abstract rules. Comput. Vis. Sci. **1**(1), 41–52 (1997)
27. Schöberl, J.: C++11 Implementation of Finite Elements in NGSolve. ASC Report 30/2014, Institute for Analysis and Scientific Computing, Vienna University of Technology (2014)
28. Shuyu, S., Riviere, B., Wheeler, M.: A Combined Mixed Finite Element and Discontinuous Galerkin Method for Miscible Displacement Problem in Porous Media. In: Recent Progress in Computational and Applied PDES, pp. 323–351. Springer US (2002). https://doi.org/10.1007/978-1-4615-0113-8_23
29. Stenberg, R.: Postprocessing schemes for some mixed finite elements. ESAIM: M2AN **25**(1), 151–167 (1991). https://doi.org/10.1051/m2an/1991250101511
30. Wheeler, M., Yotov, I.: Mixed finite element methods for modeling flow and transport in porous media. pp. 337–357. World Scientific Singapore (1995). https://doi.org/10.1142/9789814531955
31. Zhang, J., Han, H., Guo, H., Shen, X.: A combined mixed hybrid element method for incompressible miscible displacement problem with local discontinuous Galerkin procedure. Numer. Methods Partial Differ. Equ. **36**(6), 1629–1647 (2020). https://doi.org/10.1002/num.22495
32. Zhang, J., Qin, R., Yu, Y., Zhu, J., Yu, Y.: Hybrid mixed discontinuous Galerkin finite element method for incompressible wormhole propagation problem. Comput. Math. Appl. **138**, 23–36 (2023). https://doi.org/10.1016/j.camwa.2023.02.023
33. Zhang, J., Yu, Y., Zhu, J., Qin, R., Yu, Y., Jiang, M.: Hybrid mixed discontinuous Galerkin finite element method for incompressible miscible displacement problem. Appl. Numer. Math. **198**, 122–37 (2022)